THERMO-MECHANICAL CHARACTERIZATION OF CARBON-REINFORCED SHAPE MEMORY POLYMER

BY

TANMAY RAMANI

THESIS

Submitted in partial fulfillment of the requirements
for the degree of Master of Science in Civil Engineering
in the Graduate College of the
University of Illinois at Urbana-Champaign, 2017

Urbana, Illinois

Adviser:

Professor Bassem Andrawes

ABSTRACT

Shape memory materials (SMM) are those materials that possess the inimitable quality of remembering their shapes. They recover their original shapes upon exposure to external stimulus like heat, light, electric field, magnetic field, moisture etc. Types of SMMs include shape memory alloys (SMAs), shape memory polymers (SMPs) and shape memory ceramics. The most well-known and widely used SMMs are shape memory alloys. They have exceptional strength and shape memory characteristics with the most far-reaching applications. SMPs though have several advantages over SMAs and other shape memory ceramics. Few of those could be termed as light weight, low cost, good process ability, high deformability, high shape recoverability, soft texture and adjustable switching temperature. This work incorporates the manufacturing and use of polyurethane based shape memory polymers obtained from SMP Technologies, Inc. The study investigates the effect of adding carbon fiber fabric layers on mechanical properties of the pure polyurethane based SMPs. The SMP is thermo-mechanically characterized for its transition temperature (T_g) using Differential Scanning Calorimetry (DSC) and Dynamic Mechanical Analysis (DMA). Fold-deploy shape memory tests are conducted to obtain shape memory parameters like shape fixidity (or retention) and shape recovery. In addition, effect of shape recovery at different temperatures, T_g, T_g+15, T_g+30 is also investigated to examine the effect of temperature increase in recovery ratio of the samples.

Furthermore, static uniaxial tensile tests are performed to evaluate the mechanical properties of carbon reinforced SMP with focus on three important parameters vis-a-vis Young's Modulus, Tensile Strength and Tensile Strain at break. The samples are also analyzed if the samples undergoing single or multiple cycles of deformation and recovery

had any effects on its mechanical properties. Finally, the effect of degree of deformation ranging from 45˚ bend to 135˚ bend is also studied for both pure SMPs and carbon fabric reinforced SMP samples (SMPC). Four-step shape memory cycle characteristics are also verified by conducting full scale finite element studies. The results indicated glass transition temperature for the manufactured SMP to be 62˚C, with excellent shape fixidity (99%) and shape recovery (98%) ratios. In addition, mechanical testing indicated considerable improvement in stiffness and strength of the composites compared to pure SMP (nearly 100% rise with 2% fiber volume fraction). These carbon reinforced composites could potentially be used for manufacturing structural components with insignificant loss of strength or stiffness after experiencing a number of characteristic shape memory cycles. Furthermore, the loss in strength/stiffness is independent of the high deformation angles in the shape fixidity step.

ACKNOWLEDGEMENTS

I wish to extend my deepest appreciation to my advisor, Dr. Bassem Andrawes for his support throughout my graduate studies at the University of Illinois. I am thankful for his patience through my growing pains as a researcher and for the invaluable skills I have developed as a result of his guidance. Thank you to all of those in the CEE Machine Shop, namely Timothy Prunkard and Donald Marrow for your hard work which made this research possible. I would also like to express my sincere thanks to Hang Zhao, PhD candidate at UIUC, for guiding me time and again throughout my project work with his valuable expertise and knowledge in my field of work. I thank him for patiently answering all my queries, however naive they were. And especially I want to thank Rishabh Singhvi, MS Candidate at UIUC, for his valuable and generous guidance with ABAQUS software learning. I owe my deepest gratitude to my parents and brother, for always being supportive throughout my life. I am thankful for the invaluable love and encouragement they have given to me.

TABLE OF CONTENTS

CHAPTER 1: INTRODUCTION

1.1 RESEACH MOTIVATION

Nature is full of instances with materials changing shapes in response to the fluctuations in their immediate environment (Liu & Urban, 2010). Be it the case of sunflower opening its petals in response to sunlight, opening and closing of Venus flytrap to capture prey or the color change enabled by small changes in the skin layers of cattle fish, biological intelligence is not a new phenomenon (Zhao et al., 2015). Likewise, there exist special functional polymers that have something unique to offer in terms of functionality. They have been the gauge of interest for quite some time. Shape Memory Polymers (SMP) are one such materials. They belong to a special class of materials viz. smart materials, particularly, to a subclass widely known as Shape Changing Polymers, which change the shape (or so does it appear macroscopically) in response to an external stimulus (Behl & Lendlein, 2007) like temperature (Chung et al., 2008; Gall et al., 2005; Lendlein & Kelch, 2002; Liu et al., 2007; Mather et al., 2009; Yu et al., 2011), magnetic field (Buckley et al., 2006; He et al., 2011; Kumar et al., 2010; Mohr et al., 2006; Schmidt, 2006), light (Jiang et al., 2006; Koerner et al., 2004; Lendlein et al., 2005; Li et al., 2003; Scott et al., 2006), water (Chae Jung et al., 2006; Huang et al., 2005), etc. This feature of shape memory polymers is known as Shape Memory Effect (SME). Since this process involves change of shapes between two primary shapes (temporary and permanent) this effect is often termed as dual shape memory effect. The dual SME is illustrated in Figure 1.1.

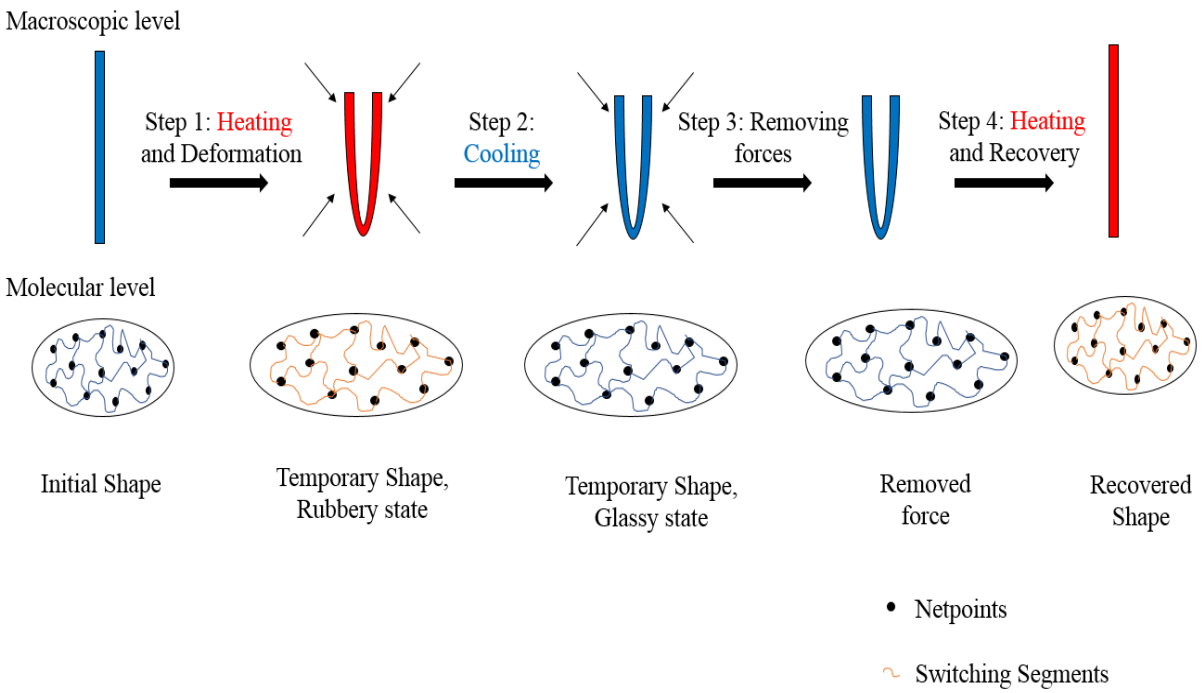

Figure 1.1: Schematic showing dual SME in shape memory polymers

This exclusive SME property of these materials brings them on the forefront of materials to be used for numerous applications. Compared to other functional materials like electroactive polymer (EAP) or PZT, SMP is easier to process. Moreover, the ease of manufacturing, faster recovery rate, low cost and light weight properties of SMP over shape memory alloys have led to their rapid development and commercialization (Leng et al., 2011; Liu et al., 2007). Until now, SMPs have had their share in wide ranging applications. It has been extensively used in medical field with the development of ophthalmic devices and its use in orthopedic surgery (Sokolowski et al., 2007). Biomedical sector has also greatly benefitted from its usage (Buckley et al., 2006; Gomes & Reis, 2004; Lendlein & Langer, 2002). Several industrial applications have also found their way with the development of shape adaptive grips, auto choke elements for engines etc. (Langer & Lendlein, 2002).

Various types of polymers have known to be exhibiting shape memory characteristics including epoxy based, cross-linked PE, cross-linked ethyl vinyl acetate polymer (Arnebold & Hartwig, 2016). Out of the wide-ranging list, polyurethane (PU)-based SMPs (SMPU) have known to be advantageous on several fronts ranging from high shape recoverability, structure designability, wide range of glass transition temperature, and better biocompatibility (Zhao et al., 2015). SMPUs essentially exist in either rubbery state or glassy state depending on the surrounding temperature. On a molecular level, it consists of rigid net points interlinked via flexible switching segments (or chains) (see Figure 1.1). Net points determine the permanent shape and switching segments are responsible for fixing the temporary shape. On heating above its characteristic temperature (glass transition temperature, T_g; melting transition temperature, T_m; or less frequently used liquid crystal clearing temperature, T_{cl}) it becomes more flexible and easy to stretch/bend/curve. This flexibility is attributed majorly to the increased mobility of molecular chains. On the other side of the spectrum, below its transition temperature, it behaves as rigid plastic material and does not deform till sufficiently high loads are applied.

Although SMPs have been used extensively for several engineering applications, their application in structures has been limited due to their low strength and stiffness. Little effort has been done to explore broadening the structural application of SMPs within the realm of improving their mechanical properties. Adding reinforcing fibers did show possibility of improved stiffness in SMP (Liang et al., 1997; Ni et al., 2000), but the field has been dormant lately. This work is focused on further exploring enhancing the mechanical characteristics of polyurethane based SMP through the use of carbon fiber reinforcing fabric to form a carbon-based SMP composite (SMPC). The study characterizes

the thermo-mechanical properties of SMPC using dynamic mechanical and static tensile testing. The shape retention and recoverability of both SMP and SMPC are also investigated through a series of fold-deploy tests.

The objectives of this research are to:

- Develop shape memory polymer at laboratory scale and characterize it for its transition temperature and shape memory properties.
- Study the thermo-mechanical properties of shape memory polymer and shape memory polymer composites for potential applications in structural components.
- Determine the most effective scheme to phenomenologically model shape memory cycle characteristics using ABAQUS.

1.2 THESIS OUTLINE

This thesis presents the experimental and analytical research findings of the thermo-mechanical characterization study of unreinforced and carbon reinforced shape memory polymer performed at the University of Illinois at Urbana-Champaign (UIUC). Chapter 1 provides the motivation and background for this study.

Chapter 2 presents an overview of literature relevant to the research interests of this study. This includes more information on characteristics of shape memory polymer, shape memory polymer composites, and research on the applications of reinforced shape memory polymer in structural engineering and other associated applications.

Chapter 3 presents experimental trial results of different methods adopted to synthesize shape memory polymer specimens in the laboratory. Different techniques used

are listed in detail along with final preparation steps used to manufacture shape memory polymer and shape memory polymer composite.

Chapter 4 presents the results of the characterization studies performed to thermally characterize the shape memory polymer. This includes information on the Differential Scanning Calorimetry (DSC) and Dynamical Mechanical Analysis (DMA) studies to obtain the transition temperature. Fold-deploy test results are presented which were used to obtain shape memory parameters like shape memory retention and shape memory recovery.

Chapter 5 outlines the development of different finite element models to study shape memory polymer behavior using ABAQUS (Dassault Systèmes 2014). This model is used to perform studies to phenomenologically model the four-step shape memory cycle characteristics to determine the most effective modelling scheme for shape memory parameters.

Chapter 6 outlines the static tensile testing results conducted on shape memory polymer and shape memory polymer composites to obtain their mechanical characteristics. Also, presented are the results on studies conducted to study the effect of bending deformation on mechanical properties under one and multiple shape memory cycles. Effect of different bending deformation angles on mechanical characteristics of SMP and SMPC is also studied in greater detail.

Chapter 7 summarizes the important findings of these experimental and analytical studies.

CHAPTER 2: LITERATURE REVIEW

2.1 SHAPE MEMORY MATERIALS

Shape Memory Materials are those materials that have the unique capability of recovering their permanent shapes upon contact with external simulation such as heat, electricity, moisture and light (Zhao et al., 2015). Various forms of shape memory materials include shape memory alloys (SMA), shape memory ceramics and shape memory polymers (SMPs). SMAs were the first to be used extensively around 1980s while the other two forms came into eminence around 1990s (Hu, 2013; Hu et al., 2012).

Shape Memory Alloys are the most used and widely accepted form of shape memory material owing to its high recovery stress, high strength and varied applications in different industries. They were first discovered back in 1930s. Au-Cd was the first alloy that was discovered to have these properties (Chang & Read, 1951). The momentum however gained prominence with the discovery of Ni-Ti based alloys, also called nitinol (Cai et al., 2005; Gu, 2013). The major advantage of these alloys came from their exceptional properties with high accuracy in glass transition temperature and huge recovery force (or stress) that is produced under the constrained recovery. These days wide variety of those are being used in various forms such as In-Ti, Cu-Zn and ternary alloys like Ni-Ti-Nb and Ni-Mn-Ga (Schetky, 1994).

The SMAs have found applications in many industries such as biomedical, electronics, and automobile industries. The SMA product range is very diverse and covers many inventions such as couplers and fasteners (Dong et al., 2001; Duerig et al., 1990; Wang et al., 2005), pace makers, bone fixing staples, stents, guide wires (Miyazaki, 1999; Otsuka & Ren, 1999; Stice, 1990) antenna, micro actuators, and sensors, anti-choking

systems (Hannula et al., 2006; Yoneyama & Miyazaki, 2008). Research over the years has proven several advantages of SMAs like very high elastic modulus, e.g., 80 GPa, excellent temperature resistance properties, easy and gradual deformation at the application temperature, very high recovery stress in a very short time (Nguyen et al., 2008), ranging from 150-400MPa, large shape recovery ratios up to 99%. On the other end of spectrum, there lies several demerits that prevent their extensive usage in many applications like high manufacturing cost, low recoverable strains usually ranging from 1-2% with the maximum 10% (Lagoudas, 2008). Thus, shape memory polymers fir precisely in those scenarios where shape memory properties are required to be used but SMAs due to aforementioned properties can't be well used.

Shape memory ceramics (SMCs) are yet another such stimuli responsive materials, the difference lies in the activation of shape memory effect in them. Essentially, electric field is used for the activation of shape memory effect in them. Piezoelectricity or ferroelectricity is the term used, in which a two-directional electricity-strain relationship exists (Valasek, 1921). Some of the well-known ceramics demonstrating SME are barium titanate ($BaTiO_3$), which is also the first piezoelectric ceramic discovered, lead titanate ($PbTiO_3$), lead zirconate titanate ($Pb[Zr_xTi_{1-x}]O_3$) ($0<x<1$) (known as PZT and the most frequently used commercially available piezoelectric ceramic), potassium niobate ($KNbO_3$), sodium tungstate (Na_2WO_3) (Jaffe, 2012).

The applications of SMCs are very much diverse and mostly concentrated in the areas of actuators, sensors, and energy generation from motion. The most famous applications include sonar detectors in submarines, lighters, energy generation from motion, transducers, and vibration detectors (Pons et al., 2007; Wax et al., 2003).

SMPs although less explored compared to SMAs, have several advantages over their SMA counterparts like low cost, light weight, high shape fixidity and recoverability, superior deformation levels, ease of manufacturing and the ability to adjust or tailor the transition temperature thermo-mechanically. They are detailed in further detail in the next section.

2.2 SHAPE MEMORY POLYMERS

Shape memory polymers (SMP), sometimes lightly referred to as smart polymers or more scientifically stimuli-responsive polymers have the ability to recover from temporary shape to permanent shape on exposure to external stimuli (Liu & Urban, 2010). This is quite in resemblance to the biological intelligence observed in the nature. SMP belong to a wider class of materials widely termed as Shape Changing Polymers (SCPs) (Zhao et al., 2015). Whereas macroscopic changes in polymer functions are often accompanied by chain conformational changes (i.e. shape changes at the molecular scale), stimuli-responsive shape changing polymers (SCPs) commonly refer to those for which shape changes are either macroscopic or at least visible under microscopes. The differentiating behavior that sets the SMP apart from other shape changing polymers is the feature termed as programmability. Programmability is the process or the procedure adopted that essentially involves the application of external (generally, physical in nature) force or stress that defines the shape shifting pathway. This process is independent of how the material is prepared or fabricated in the first place. SMPs fall under this special category of Shape Changing Polymers which can be programmed after the fabrication step to determine the temporary fixation step to recover back subsequently to the original

permanent shape upon stimulation (mostly heating). As is evident that this whole process of fixation and recovery involves two basic shapes, one temporary and other permanent, this phenomenon is referred to as dual shape memory effect (SME) representing the most common and well known SMPs. The most well-known examples for the non-programmable type of shape changing polymers include swelling/deswelling of hydrogels (Qiu & Park, 2001) to the intriguing reversible surface morphological changes of liquid crystalline elastomers (LCEs)(Yang et al., 2006). Figure 2.1 illustrates the common classification of shape changing polymers as described in the paragraph above.

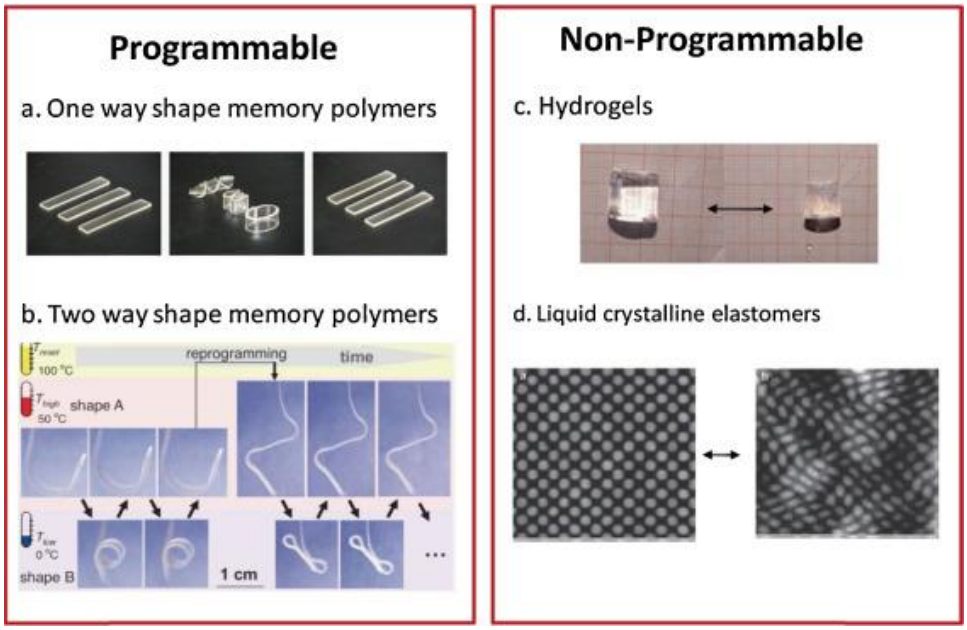

Figure 2.1: Classification of shape changing polymers (Zhao et al., 2015)

The shape memory behavior shown in Figure 1.1 is typically termed as thermally induced one-way dual shape memory behavior for the polymer in its most neat form. Thermally induced refers to the mode of stimulation that is used in activating the polymer. One-way refers to the irreversible shape-shifting behavior, i.e. the phase transformation takes place from temporary shape to permanent shape and the reverse case scenario is not

possible. Dual shape memory behavior refers to the number of shapes involved in the process, here the case being two, one intermediate after the shape fixidity step (temporary shape) and one original or permanent shape that is started from. However, SMPs can exist in many different permutations and combinations of the same. The mode of activating the shape memory behavior can also be electrical (Asaka et al., 1995), moisture (Chae Jung et al., 2006) and even magnetic (Mohr et al., 2006). The tunability of shape memory polymers also in a way help program SMPs where more than one intermediate shape exists, termed as multi SMPs. Similarly, SMPs need not only be one-way and can be 2W-SMPs also. On similar lines, the SMP need not be in its purest / neat form, it also exists in the gel or the composite forms. Figure 2.2 illustrates a schematic example of one-way dual shape memory polymer and one-way triple shape memory polymer (with two metastable intermediary shapes and one equilibrium (permanent) shape).

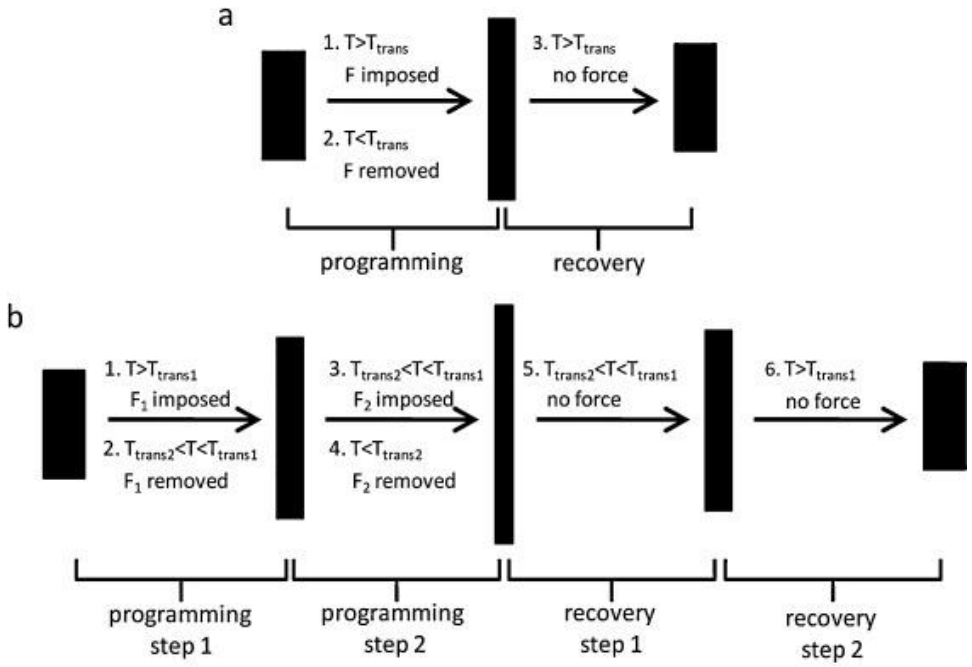

Figure 2.2: Dual and Triple Shape Memory Effect (Zhao et al., 2015)

Though, in more traditional terms SMPs have been classified into chemically (or physically) crosslinked glassy (or semi-crystalline) polymers (Lendlein & Kelch, 2002;

Xie, 2011). This classification is mostly related to the thermal phase transitions that occur in the shape memory polymer. More recently though, reversible molecular phases are more prominent in vast comparison to reversible switches (Hu et al., 2012).

2.2.1 Molecular Mechanism of SMPs

The shape memory behavior just described in previous sections can also be fundamentally explained from the molecular stand point. The case of thermally induced, one-way shape memory polymer is taken to elaborate the mechanism of shape memory effect. As shown in Figure 2.3 (black dots: netpoints; blue lines: molecular chains of low mobility below T_{trans}; red lines: molecular chains of high mobility above T_{trans}), at the microscopic level, the shape memory polymer consists of switching segments (or chains) that undergo conformational changes and network points that maintain the network. At temperatures below the transition temperature, T_g (or melting temperature; T_m, or crystallization temperature; T_{cl}) the material is very rigid, whereas going past that temperature, the material becomes considerably softer, essentially behaving like a rubber (or elastomer) which can be molded to any desired shape. The material deformed at this temperature is more commonly described as deformation temperature (T_d). At the molecular level this observed phenomenon is explained via slackening or loosening of molecular chains. With the application of externally applied force or stress, a metastable intermediary shape is fixed, while the temperature is lowered, principally locking the shape. The temperature at this fixation step is termed as shape fixing temperature (T_f). The mobility of the chains is the lowest at this point, effectively in a completely restrained position that doesn't allow any movement. The permanent shape which is also the

equilibrium shape gets restored when the polymer is again heated past the transition temperature. Again, at the molecular scale, heating activates the molecular mobility, which releases the entropic energy, thus driving the molecular chains back into its highest entropic state corresponding to the permanent shape (Zhao et al., 2015).

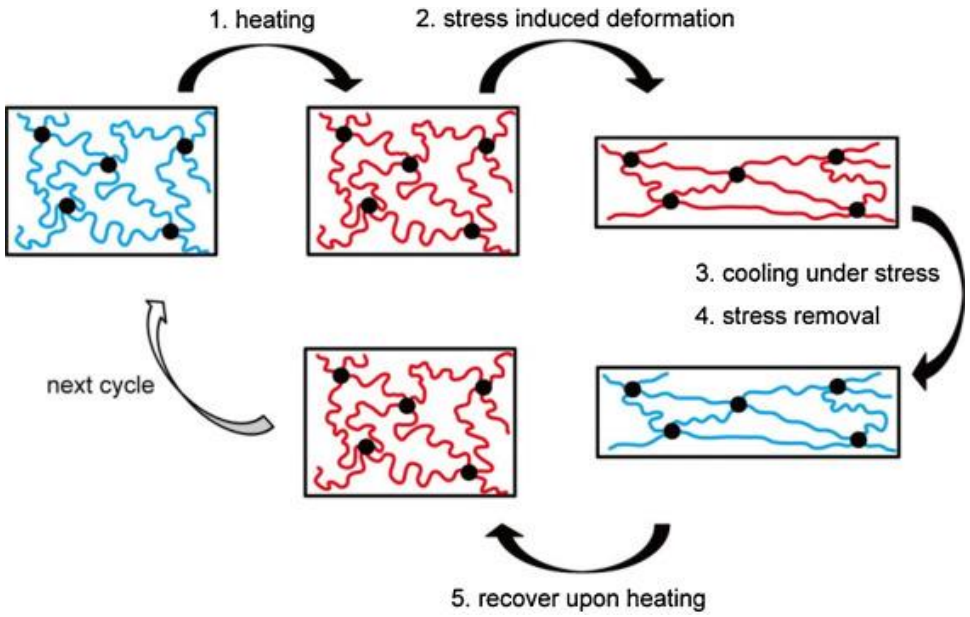

Figure 2.3: The molecular mechanism of the dual-SME (Zhao et al., 2015)

2.3 SHAPE MEMORY POLYMER COMPOSITES

Pure SMPs, severely lack many properties that make them unsuitable for various functions, specifically that require high mechanical properties, like high stiffness and strength, or for that matter high recovery force, good electrical conductivity and self-healing properties. Therefore, lately research on shape memory polymers has shifted base to develop shape memory polymer composites to study in greater detail their mechanical and other thermo-mechanical characteristics to meet as desired requirements in varied application areas. On a very fundamental level, polymer composites polymer composites

are an amalgamation of a polymer matrix and filler materials such as particles, fibers, platelets or tubes, where the size of filler material varies from micro to nano scale usually (Lendlein, 2010). The matrix or the host in this case, i.e. the shape memory polymer binds the filler together and essentially protects them from damaging by uniform distribution of stress within the whole specimen. This unique interaction between the host and filler creates an interconnected network which in turn enhances material properties and create novel functionalities that are non-existent otherwise. The development of shape-memory polymer composites (SMPCs) enables high recovery stress levels as well as novel functions such as electrical conductivity (Liu et al., 2008; Lu et al., 2007), magnetism (Ding et al., 2008; Kommareddi et al., 1996), optical functions (Ravindranath et al., 2006; Sainz et al., 2006) and biofunctionality (Chiellini et al., 2008; Costantino et al., 2009).

The filler materials that have been used in the past decade to develop shape memory polymer composites can be categorized into three main categories, explicitly particles, of filler materials could be found, namely particles (e.g., silica, metal, polyhedral oligomeric silsesquioxanes (POSS), and other organic and inorganic particles), layered materials (e.g., graphite and layered silicate), and fibrous materials (e.g., nanofibers and single-walled and multi-walled nanotubes). These three types are as illustrated in Figure 2.4 with an important morphological characteristic that describes the surface area to volume ratios.

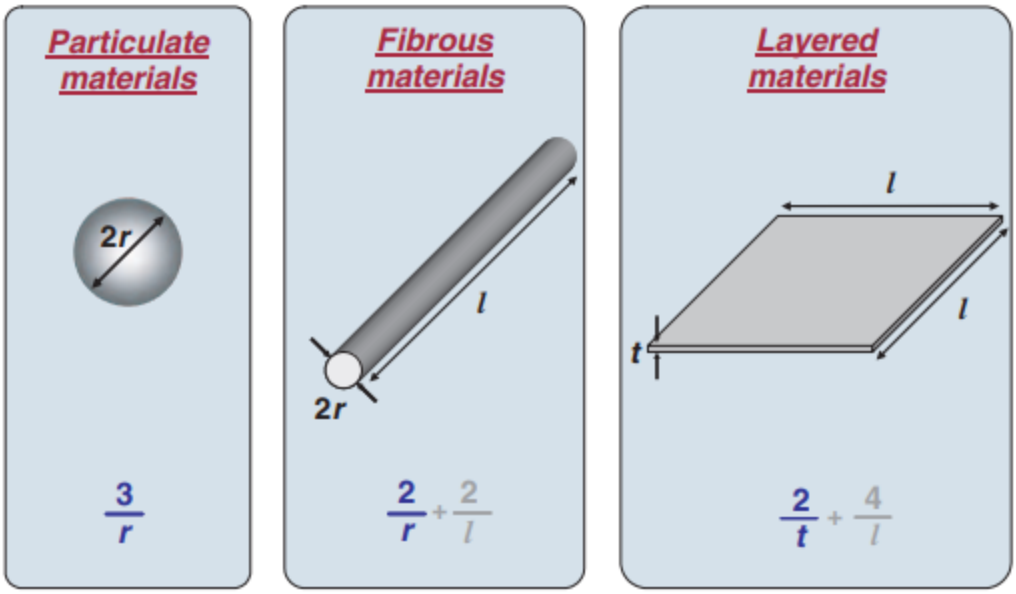

Figure 2.4: Surface/volume (S/V) ratios for varying filler geometries, r is the radius, l is the length, and t is the thickness of filler (Hussain et al., 2006)

As stated previously, for the case of shape memory polymers, with light weight, low cost of preparation, easy manufacturability and high recovery strain (compared to their SMA counterparts), they still possess very less recovery stress (2-3MPa) compared to very high in the case of shape memory alloys (0.5±0.25GPa) and inferior stiffness and strength values (Mondal & Hu, 2006). Different types of fibers ranging from micro-nano scale have been added to increase the stiffness and strength characteristics of the polymer, namely carbon glass and Kevlar fibers. Depending on the type of fibers used, varied level of enhancement in properties has been obtained for different polymer blends. For e.g. for the case of shopped fibers like carbon, 40-50 % wt. was required to obtain the necessary improvement in polymer stiffness whereas for its nano size counterpart like SiC for example improved the constrained bending force recovery by 50 % compared with neat polymer by its mere addition of 20% by wt (Wei et al., 1998). On the other hand, with the addition of fibers, the recovery strain has been shown to decrease considerably in addition

to ultimate strain limit due to the limiting strain carrying capacity of filler fiber materials added. It has been reported a loss of shape recovery rate from 98 % to 65 % with the addition of 30 % by weight of carbon black to a polyurethane based SMP (Gall et al., 2002).

Interestingly, out of all the filler materials that have been added to different shape memory polymer mixes, carbon nanotubes have excelled in improving the properties due to their terrific mechanical, thermal and electrical properties. Superior mechanical properties have been reported due to addition of carbon nanotubes (CNTs) by different researches over the last few years (Cadek et al., 2002; Coleman et al., 2006). In addition, superior stress and strain recovery characteristics have also been observed for SMP blends with carbon nanotubes. Despite all the benefits as mentioned above, dispensability of the CNTs in the polymer mix has been a constant source of complexity in manufacturing these polymer mixes. Although it has been reported that the compatibility and homogeneous distribution of CNTs could be obtained by surface modification in nitric acid and sulfuric acid mixture and several other related techniques, the process still remains tedious at the least. Recently, cup stacked carbon nano tubes (CSCNT) have been reported to gain momentum with exemplary advantages over single-walled carbon nanotubes (SWCNTs) and multi-walled carbon nanotubes (MWCNTs) (Endo et al., 2003a; Endo et al., 2003b; Hasobe et al., 2007). Their unique morphology with hollow core and large portion of open ends offer better interphase and interaction properties with the surrounding polymer properties and hence significant improvement in mechanical properties (Endo et al., 2003a). It was observed that isothermal mechanical tests conducted on CSWT reinforced polymer indicated the elastic modulus, tensile strength and flexural strength increased by 61 %, 66 % and 84 % respectively with mere 2 % reinforcement. Also, the glass transition temperature

of SMP composite decreased from 61.9˚C to 52.8˚C by embedding 2 wt.% of CSCNTs, indicating that the shape recovery process could be triggered more easily by external stimulus due to the role of reinforcement fillers (Yu et al., 2014).

Also, noticeable is the fact that not only is the development in terms of mechanical properties is obtained via addition of fibers, but new functionalities are introduced to the shape memory polymers vis-à-vis conductivity, electrical and magnetic facilities bio functionality depending on the type of fiber used for the study. Specifically, for the conductivity, fillers such as carbon black (CB), carbon fibers, carbon nanotubes, or graphite which are highly conductive materials have shown to contribute significantly to make conductive polymers. These carbon-based compounds have significantly lower electric resistance and the resulting SMPC are highly conductive in nature which could be triggered by the means of joule heat as an indirect method of actuation (Lendlein, 2010). (Leng et al., 2008) investigated the electrical and thermomechanical properties of a SMPC containing carbon black nanoparticle and short carbon fiber of 0.5-3mm length and 7μm diameter. These filler materials together in conjunction greatly improved the conductivity of the material. Figure 2.5 shows the shape memory cycle for SMP/CB/SCF composite.

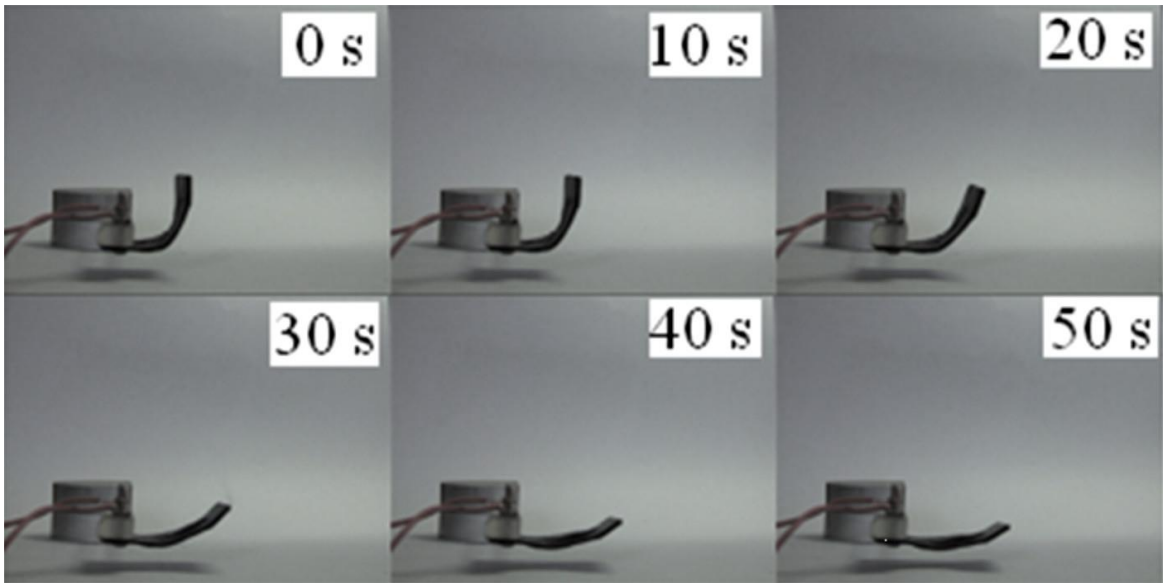

Figure 2.5: Series of photographs showing the macroscopic SME of SMP/CB/SCF composite containing 5 wt% CB and 2wt% SCF (Leng et al., 2008)

Similarly, Magnetically-induced SME for composites from thermoplastic SMPU and aggregated micro-sized Fe_3O_4 particles for different particle contents up to 40 vol.% was reported (Yang et al., 2005). The magnetic particles were mechanically mixed with the SMPU at 200˚C for 10 min. Alternating magnetic field with a frequency of 50Hz and a magnetic field strength of 4.4kAm^{-1} were employed to induce the SME. Under this condition a programmed helically bended stripe consisting of SMPU and 20 vol.% magnetic particles recovered to its original plane stripe shape within 20min. Similarly, other studies like have looked into various thermo-mechanical property enhancements with magnetically induced shape memory polymer composites.

The current study in particular looks into developing carbon fiber fabric composites much like the composite laminates to improve the stiffness and strength characteristics of a polyurethane based SMP for potential applications in structural engineering applications which has yet remained unexplored.

2.4 STRUCTURAL APPLICATION OF SHAPE MEMORY POLYMER COMPOSITES

SMPs have some drawbacks, such as low strength, low stiffness, and low recovery stress. Therefore, the need for development of fiber-reinforced shape memory polymer composites came into being to satisfy the ever-increasing strength and stiffness demands of the composites with shape memory properties. Microelectromechanical systems, surface patterning, biomedical devices, aerospace deployable structures (Liu et al., 2014), and morphing structures (Chen et al., 2014) are various dimensions where the SMP composites have either been studied lately or currently being explored. In order to light the weight and reduce the mechanical complexity of the inflatable structure system, Li et al. (2016) have designed and analyzed a cubic deployable support structure based on SMPC preliminarily. The cubic deployable support structure performs high packaging efficiency for launch, self-deployment without complex mechanical devices and can improve the robustness of the inflatable structure system. The cubic deployable support structure based on SMPC consisted of four dependent spatial cages, each spatial cage is composed of 12 three-longeron SMPC truss booms and end connections as shown in Figure 2.6.

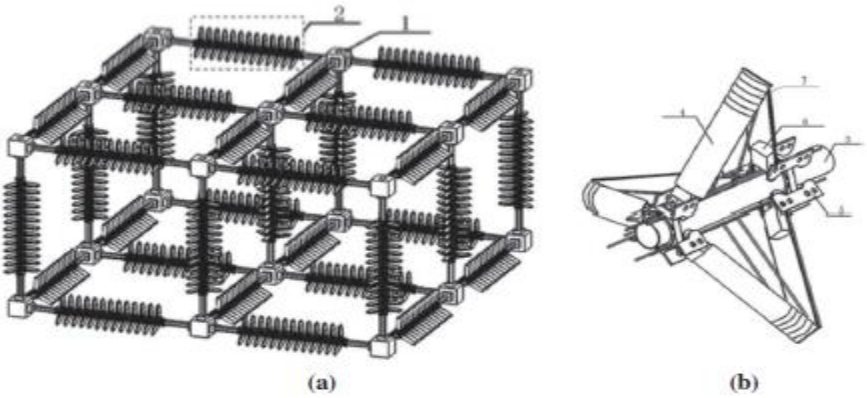

Figure 2.6: (a) Cubic deployable support structure, (b) three-longeron deployable laminates unit, 1 –end connection, 2 – three-longeron SMPC truss boom, 3 – extendable central bracket, 4 – arc shaped deployable laminate, 5, 6 – connectors, 7 – resistor heater. (Li et al., 2016)

Also, Takeda et al. (2015) investigated and presented findings on flexural stiffness controllability of hybrid beams and woven carbon fiber reinforced polymer (CFRP) composite and SMP layers. Flexural tests were conducted on the layered cantilever beams to evaluate the dependence of the beam flexural stiffness on the temperature. In addition, electrical resistive heating of the woven CFRP layers was employed to control the temperature of CFRP layers. Figure 2.7 shows the schematic of hybrid layered cantilever beam.

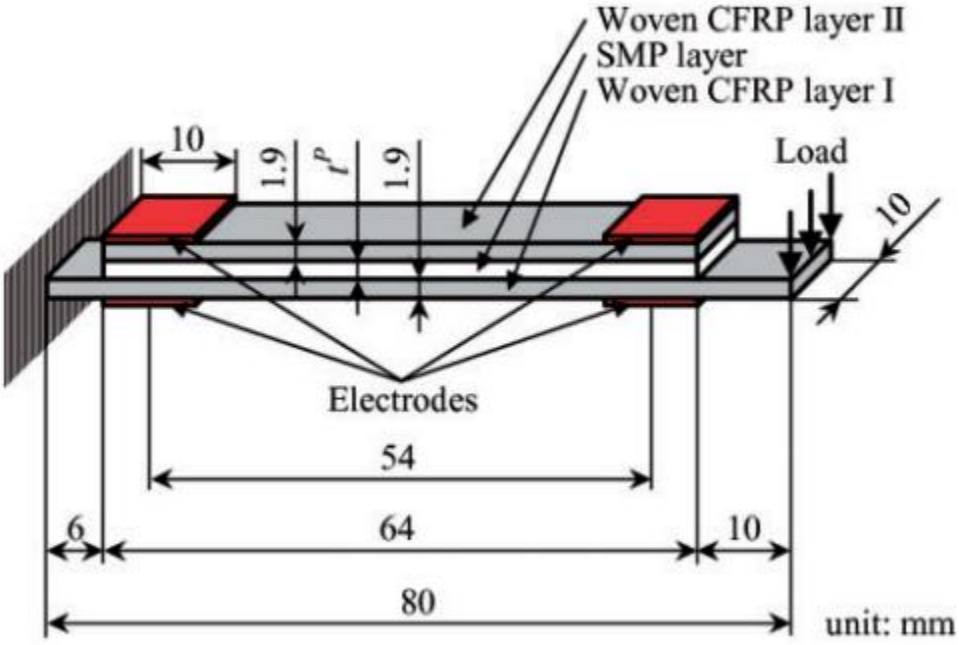

Figure 2.7: Schematic of hybrid layered cantilever beam (Takeda et al., 2015)

Also, Baghani and Taheri (2015) investigated the structural behavior of a shape memory polymer (SMP) actuator analytically. This system consisted of a reinforced SMP beam and a spring which was attached to the beam in a part of thermomechanical shape memory effect (SME) cycle.

The authors proposed that the developed analytical solution can be used as an effective and efficient tool for investigating the effects of changing any of the material or geometrical parameters on smart structures consisting of SMP beams (e.g. actuators made of SMP beams) for their design and optimization where a large number of simulations is required.

Lan et al. (2009) have developed a type of carbon-fiber reinforced SMPC hinge to actuate solar array deployment and performed an experiment to simulate the deployment process in a zero-gravity environment. Also, Yang et al. developed a new type of mesh-surface antenna deployed using SMPC tapes, as demonstrated in Figure 2.8. The structure essentially consists of six pieces of SMPC thin shell tapes, six tape linkers, six guided ribs, a steel supporter and six resistor heaters (Liu et al., 2014).

Figure 2.8: The space deployable mesh-surface antenna model: (a) deployed SMPC antenna and (b) packaged SMPC thin shells (Liu et al., 2014)

Although, as seen above, SMPC composites have been widely developed using wither short fibers or micro/nano fibers, for various applications in aerospace industry, little has been done to investigate the used of fabrics and produce laminate like composites.

This work aims at manufacturing and thermos-mechanically characterizing carbon fiber fabric reinforced shape memory polymer composite for potential structural engineering applications.

CHAPTER 3: MATERIAL PREPARATION

3.1 INITIAL TRIAL

For the current study, a Shape Memory Polymer was required that would have its glass transition temperature way outside the ambient temperature range. This is to avoid triggering of shape memory effect in shape memory polymers for field-level applications. The following raw materials were obtained to synthesize the polyurethane based shape memory polymer:

Polyol: Poly (tetrahydrofuran) glycol-650 with a molecular weight of 650 g/mol and melting temperature of nearly 16°C was obtained from Sigma-Aldrich. Figure 3.1 presents general chemical formula for Poly (tetrahydrofuran).

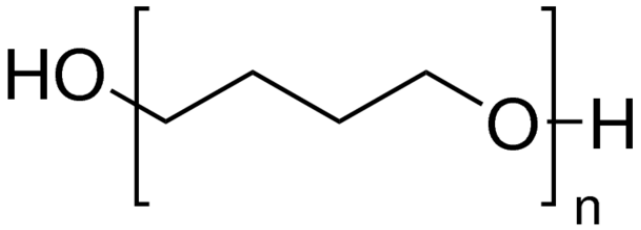

Figure 3.1: Chemical formula of Polyol

Diisocyanate: 4,4'-methylene diphenyl diisocyanate (MDI) is commercially available (MDI) and was obtained from Sigma Aldrich (USA) with a molecular weight of 250 g/mol and a melting point of 39 °C. The material was kept in refrigerator, at -10 °C with no contact with water or light, in a sealed container. Figure 3.2 illustrates the chemical formula of MDI.

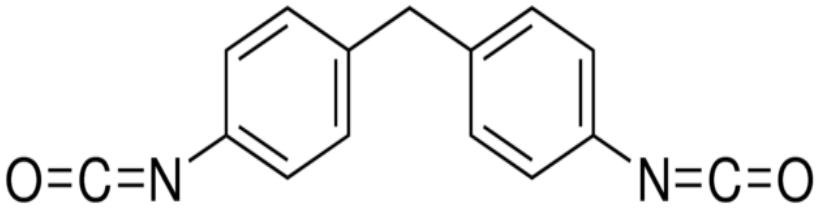

Figure 3.2: Chemical formula of Diisocyanate

Chain extender: 1, 4-butanediol (BD) with molecular weight of 90 g/mol was purchased from Sigma Aldrich, USA. These small molecular weight diols are used to increase the molecular weight of polyurethane and to enhance phase separation. Figure 3.3 demonstrates the chemical formula of 1,4-BD.

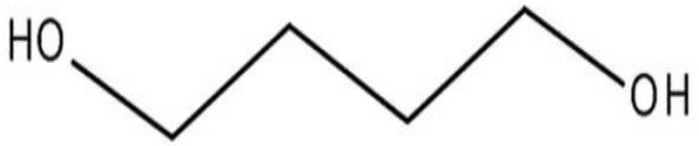

Figure 3.3: Chemical formula of 1,4- butanediol

Catalyst: Dibutlytin dilaurate was obtained in liquid form from by Sigma Aldrich, USA. Figure 3.4 below illustrates a general formula of the same

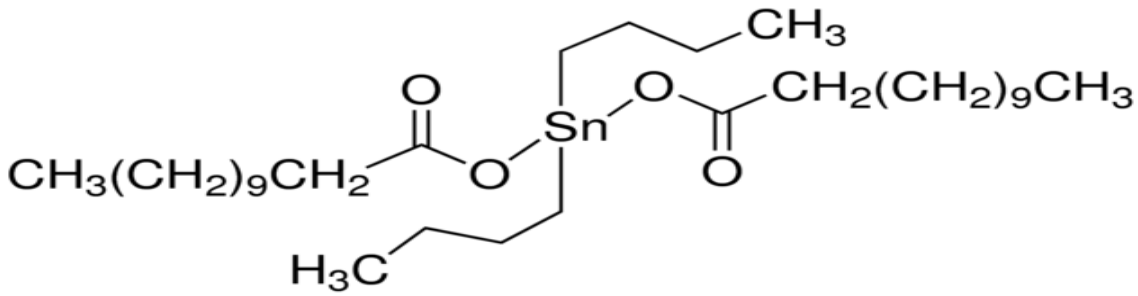

Figure 3.4: Chemical formula of Dibutlytin Dilaurate

3.1.1 Synthesis of Polyurethane System

The polyurethane shape memory polymer was synthesized by using poly (tetrahydrofuran) glycol-650 (Sigma-Aldrich) as the soft segment and Methylenebis (phenyl isocyanate) (Sigma-Aldrich) and Butanediol (Sigma-Aldrich) as the hard segments. All the chemicals were dried before use. Figure 3.5 shows the manufacturing process for the same.

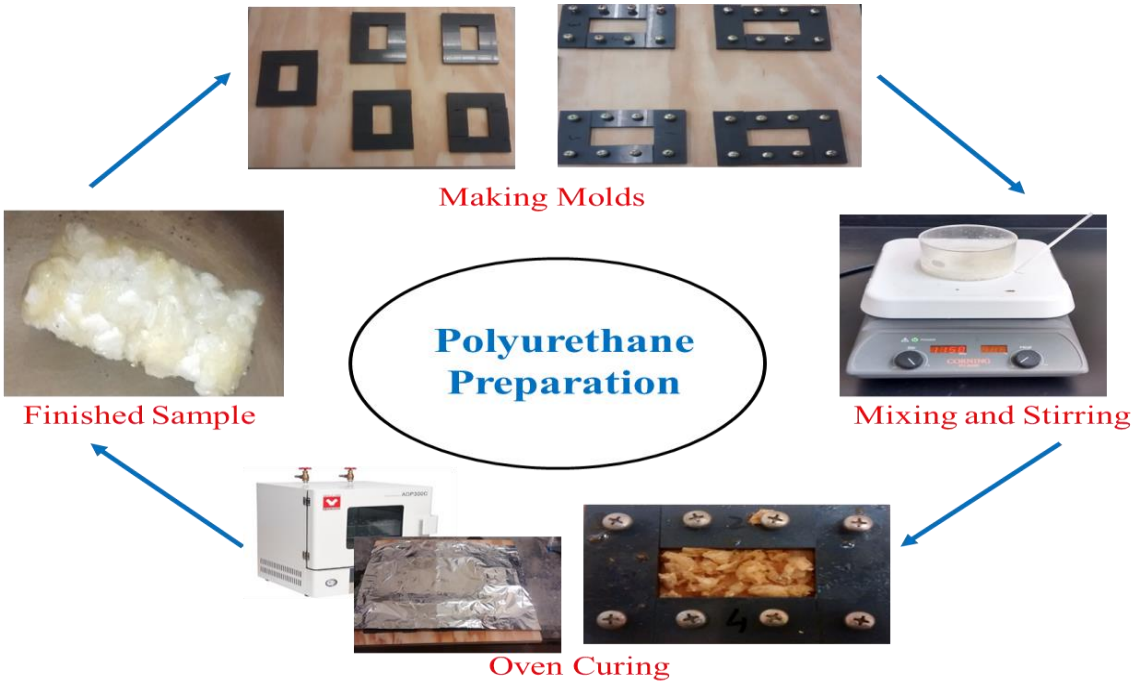

Figure 3.5: SMP Preparation Schematic

The synthesis was conducted by bulk polymerization. Dibutyltin dilaurate was used as the catalyst. The switching transition of the shape memory polymer was modified by varying the soft segment length and hard segment content. The poly (tetrahydrofuran) glycol was first reacted with the Methylenebis (phenyl isocyanate) for 20 min. Then the prepolymer was reacted with the chain extender. After about 30s of mixing, the mixture

was cast into a mold covered with polytetrafluoroethylene for further reaction. The cast mixture was cured for 12 h at 110°C by in oven. Reversible phase transformation of soft segment is reported to be responsible for the shape memory effect. Therefore, the shape memory effect could be controlled via molecular weight of soft segment, mole ratio between soft segment and hard segment, and polymerization process and can be obtained at the range of temperatures around T_g. Various trial mixes with different percentages of hard and soft segments were tried to ensure the desired shape memory properties with requisite glass transition range could be obtained. Table 3.1 shows the mol % ratios used for different trial mixes for the current study.

Table 3.1: Trial Mixes for SMP

Mol [%]			**wt. % of hard segment**
Hard Segment	**Soft Segment**	**Catalyst**	
5	1	4	45
4	1	3	40
3.5	1	2.5	35
3	1	2	30
2.5	1	1.5	25

This method of preparation was later rejected due to complexities of laboratory control involved in the process of manufacturing.

3.2 FINAL MATERIAL PREPARATION

Polyurethane based Shape Memory Polymer (SMP-5510) obtained from SMP Technologies Inc., Japan was used for the entire study. The product is potting type and

Table 3.2 ("Shape Memory Polymer Properties," 2016) enlists the basic properties of this product.

Table 3.2: Basic Properties of MP-5510

Properties	Region	Parameter	Value
Color Tone	-	-	Light yellow
A/B Weight Ratio	-	-	40/60
Viscosity(mPA·s)	-	Solution A	200-600
		Solution B	200-800
Specific Gravity	-	Solution A	1.062
		Solution B	1.215
		Residue	1.21
Strength	G/R[a]	Bending Strength (MPa)	75
		Bending Modulus (MPa)	1800
		Tensile Strength (MPa)	52
		Hardness (Shore D)	80
	R/R[b]	Tensile Strength (MPa)	20
		100 % Modulus (MPa)	4.5
		Hardness (Shore D)	40
Glass Transition Point (˚C)	-	-	55
Cure	-	Pot Life(Standard)	180 sec
		Cure Temp(˚C x time)	70˚C x 1hr-2hr

[a] G/R , Glassy Region

[b] R/R , Rubbery Region

The material obtained was in the form of two-part system, resin (A) and hardener (B). This SMP family is semi-crystalline with a degree of crystallinity of 3~50 wt. % (Hayashi, 1992). The obtained product (SMP5510) was a proprietary product of the company, produced using commonly available diisocyanate, polyol and a chain extender.

Figure 3.6 illustrates the chemical formula of the individual components and the final polyurethane product.

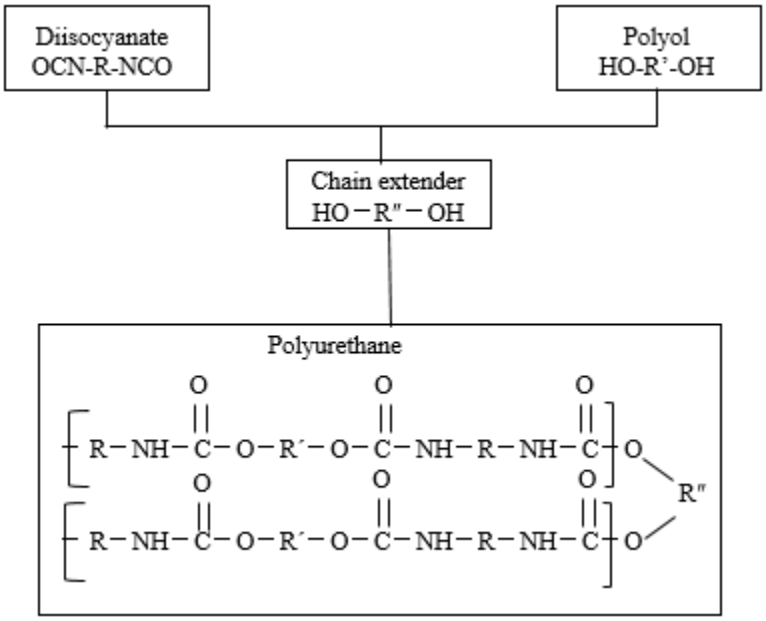

Figure 3.6: Polyurethane based SMP used in the study

3.2.1 SMP and SMPC fabrication

The fabrication process of the polymers used in the study comprised of four primary steps. The first step is the preparation step, which involves drying of liquids A and B for 1 hour at less than 50 torr pressure. The temperature is fixed at 50˚C while the components are degassed in the degassing oven. In addition, the die is dried for an hour at 70˚C. The second and the most vital step in the preparation of the product is the potting step. Herein, firstly, liquid A and B are placed in vacuum chamber of less than 50 torr. After drying, the component B (the hardener) is filtered using a mesh to remove the thin dried film formed on its surface. This helps achieve a more homogeneous mix. Then, liquids A and B are mixed in 40:60 ratio for 30 seconds with continuous stirring at the speed of 60 rpm.

Instantly after the mixing, the mixed solution is poured in the die. The vacuum is discharged immediately as the solution flows completely inside the die. The third and next important step is curing and removal. It involves removal of the die from the vacuum chamber and curing the material for 1-2 hours at 70˚C. Thereafter, finished product is removed from the die and cured for an additional 1-2 hours at 70˚C, if necessary. The fourth and final step is the cleaning step. The manufacturer recommends methylene chloride for the cleaning.

Preparation of SMPC, for most part remains analogous to SMP. Fabrics used for the current study were obtained in most part were from FiberGlast, USA with the properties as mentioned in the following Table 3.3.

Table 3.3: Product properties of carbon fiber fabric used in the study

Parameter	Type/Value
Warp Raw Material	3K-Multifilament Continuous Tow
Filling Raw Material	3K-Multifilament Continuous Tow
Weave Pattern	Plain
Fabric Area Weight	193 ± 8 gsm
Warp Ends/Inch	12.5 ± 1.0
Pick/Inch	12.5 ± 1.0
Nominal Thickness	0.012 inches
Fabric Width	50 ± 0.25/-0 inches

The difference in preparation comes after the step when the liquids are mixed. Instead of pouring the complete mixture into the die, it is half-poured, the carbon fabric is placed, coated with a brush of resin to completely infuse resin into the fiber, followed by pouring resin into the remainder of the die mould. It is then placed for curing at 70°C, as quickly as possible, owing to short pot life of the resin (180s). The schematic diagram in

Figure 3.7 summarizes the entire process for the manufacturing of SMP and its composite (SMPC).

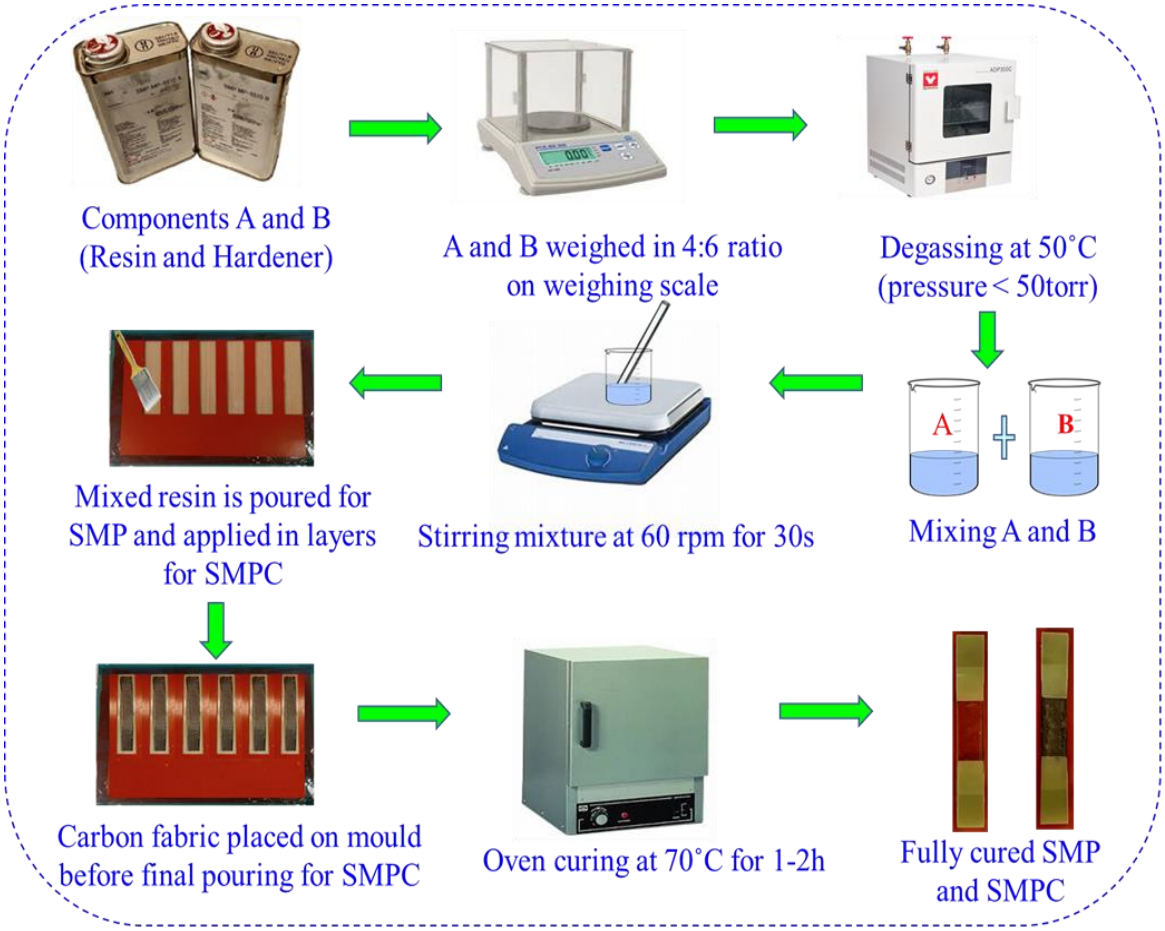

Figure 3.7: Manufacturing methodology for SMP and SMPC

CHAPTER 4: THERMOMECHANICAL CHARACTERIZATION

4.1 CHARACTERIZATION METHODS

The thermomechanical characterization methods utilized in this study can be divided into three subcategories: 1) thermal, e.g., differential scanning calorimetry (DSC) and dynamic mechanical analysis (DMA); 2) mechanical, e.g., tensile testing; and 3) geometrical, e.g. fold deploy tests to characterize shape memory properties. The current chapter covers DSC, DMA, and fold deploy shape memory tests.

4.1.1 Differential Scanning Calorimetry

DSC belongs to physical and physico-chemical methods of thermal analysis which are used to detecting thermal energy (enthalpy) changes in observed substances. The conceptual paradigm for DSC was initially determined from the theory of Differential Thermal Analysis (DTA). DTA, in theory measures the temperature difference between the sample under study and the reference sample (which does not undergo any phase change or transition) as the furnace undergoes a temperature controlled program. DSC instead of measuring the change in temperature, measures the change in enthalpy. This is primarily based on the principle that one sample and one reference are heated and cooled at a pre-specified rate and the compensated heat flux is measured that keeps the temperature of both the substances the same (Nguyen, 2012). Usually, to keep the temperatures same for the two substances, two individual heaters are used to supply heat. The experimental DSC curve shows the heat flux (mJ/s) or specific heat capacity C_p (J/gK) versus temperature.

For the current study, DSC was essentially used to determine the glass transition temperature and to determine if there was any crystallinity present in the samples. Experiments were run using a Perkin–Elmer Diamond DSC. Figure 4.1 shows the experimental setup used for the study at microanalysis laboratory facility at University of Illinois, Urbana-Champaign.

Figure 4.1: DSC Setup at microanalysis facility, UIUC

The first most important step in the process was the sample preparation. Normally the sample's weight for DSC varies from 2 mg to 5 mg. Usually, if the sample size is too little, DSC cannot detect the enthalpy change and the very purpose of DSC falters. On the other end of spectrum, if the sample is way too much, DSC becomes ineffective in the sense of thermal gradient being too high (Nguyen, 2012). Also, to be noteworthy is the fact the temperature is not homogeneous everywhere, the deepest point where the contact is the hottest point. For the current study, 5 mg samples were cut from heat and radiation crosslinked samples and placed in standard aluminum pans. The samples were loaded at room temperature. The temperature range was -20 – 200˚C, with a ramp rate of 20˚C/min and a soak time of 5 min at the end of each heating/cooling cycle. An initial ramp cycle was run for each sample to relieve thermal stress and allowed any residual solvent or

monomer to evaporate, and a second ramp cycle was run to determine T_g. As it was known prior that glass transition is below 100˚C, for the second cycles (after the first cycle removes any thermal history) the maximum temperature was restricted to 100˚C Glass transitions were determined using the Pyris software according to the half-height method. Two samples from the same batch were run through the two cycles of heating and cooling each. Figure 4.2 shows the results for sample 1.

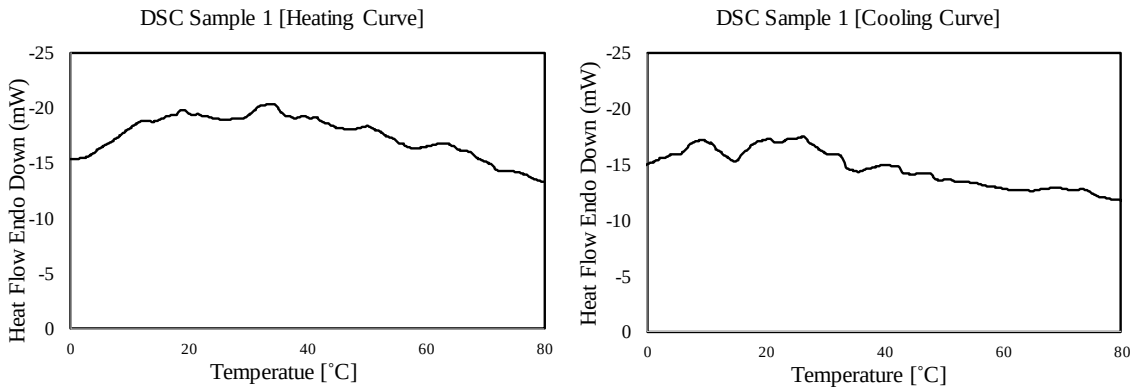

Figure 4.2: DSC Curves for Sample 1

Due to the non-crystallinity of the samples, and perhaps due to sample being not completely homogeneous, the sharp peaks around the glass transition temperature were not obtained and hence a second run was performed to get consistency in results. The weight of the sample was kept the same and the sample was run through an initial cycle ranging from -20-200˚C with a soak time of 5 minutes at the end of each terminating point and then later for the main cycle, the variation in temperature range was kept from -20-100˚C with a soak time of 10 minutes each. Figure 4.3 shows the results from the DSC analyses of the sample identity 2.

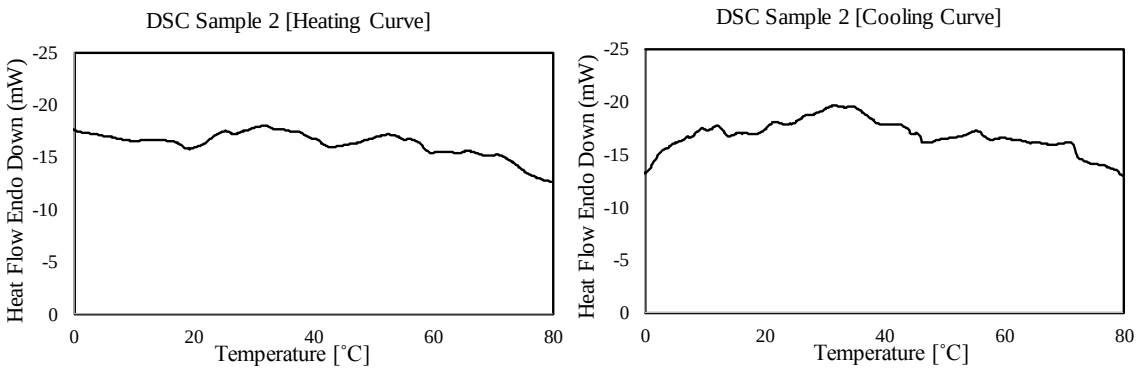

Figure 4.3: DSC curves for sample 2

Due to the fact that for the polyurethane based SMP, Differential Scanning Calorimetry couldn't give a complete transition range for the samples, the prepared samples were later thermo-mechanically characterized for glass transition by Dynamic Mechanical Analysis as described in more detail in the later section.

4.1.2 Dynamic Mechanical Analysis

Measuring the glass transition temperature (T_g) of the SMP used in this study was performed using dynamic mechanical analysis (DMA). The glass transition is associated with the motion of polymeric chains including the neighbouring segments. DMA measures the viscoelastic moduli, storage and loss modulus, damping properties, and tan delta, of materials as they are deformed under a period (sinusoidal) deformation (stress or strain) as shown in Figure 4.4 (Perkin Elmer, 2013).

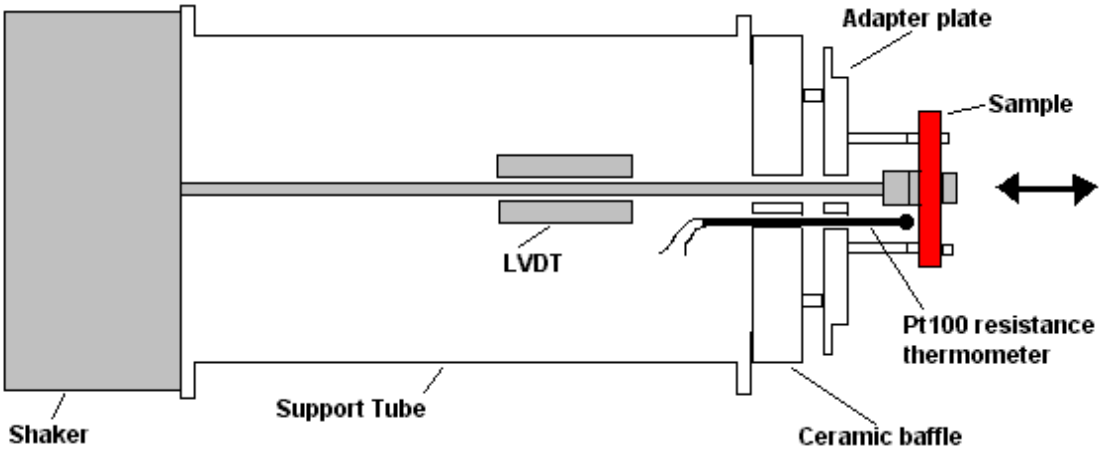

Figure 4.4: Principle of DMA (Perkin Elmer, 2013)

A sinusoidal deformation of the sample is produced by the shaker (applied load ~ STRESS) and when the material is deformed under such oscillatory stress, the material response is measured. A slightly out of phase wave is measured by the LVDT (resulting ~STRAIN)

The very basic characteristics of this response may be used to determine the elastic and viscous properties of the material. Elastic properties are measured via a parameter better known as Storage Modulus and viscous properties are determined via the parameter known as loss modulus. These properties are extremely sensitive to the glass transition as the material quickly changes nature from rigid to flexible around this temperature range. Tangent Delta is yet another parameter which is defined as the ratio of the loss modulus to the storage modulus and is a measure of the damping properties of the material. In the case of a perfectly elastic material, for example, steel, delta = 0º s shown in Figure 4.5. In the case of a perfectly viscous material, for example, water or glycerine, delta = 90º as shown in Figure 4.6.

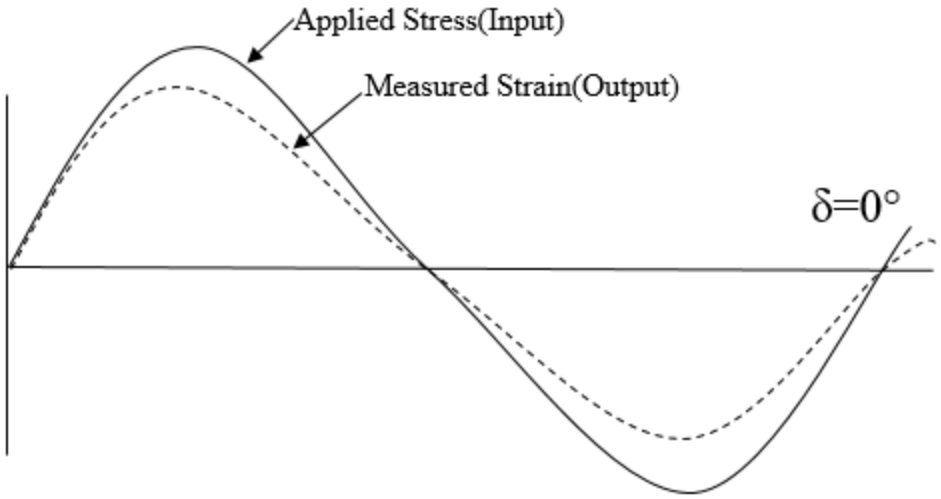

Figure 4.5: Load-response characteristics for a perfectly elastic material

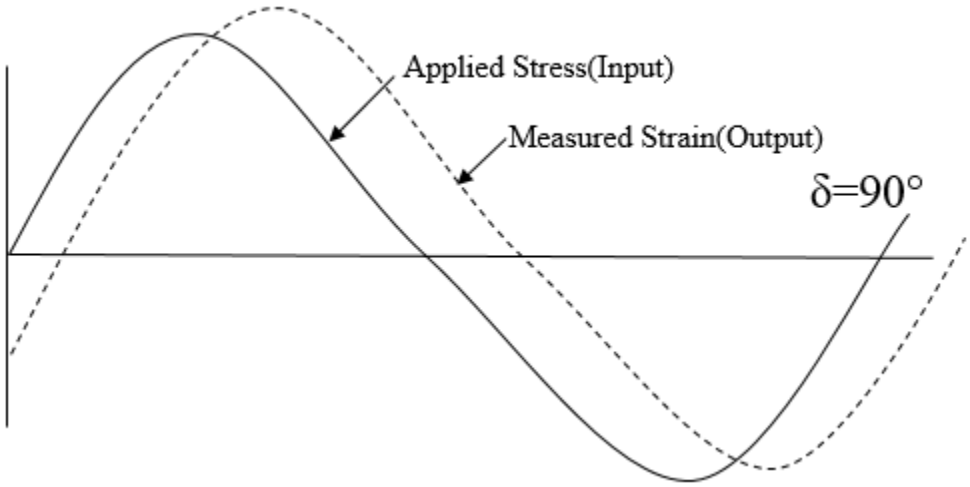

Figure 4.6: Load-response characteristics for a perfectly viscous material

For this study, tests were performed using three-point bending mode as this mode is known to work best with stiff samples. The dimensions of the samples used were 45 mm (L) x 12.55 mm (W) x 3.1 mm (T). The temperature range of the test was kept within 25˚ C and 75˚C and the loading rate for heating the sample was 1˚C/min while the unloading rate for cooling was 10˚C/min. Oscillation frequency was specified to be 1 Hz. The quantities that were kept in consideration were storage modulus, loss modulus and tanδ.

Here, tanδ, the tangent of the phase angle is the ratio of loss modulus to storage modulus. Figure 4.7 shows the setup (PerkinElmer DMA 8000) used for performing the DMA tests.

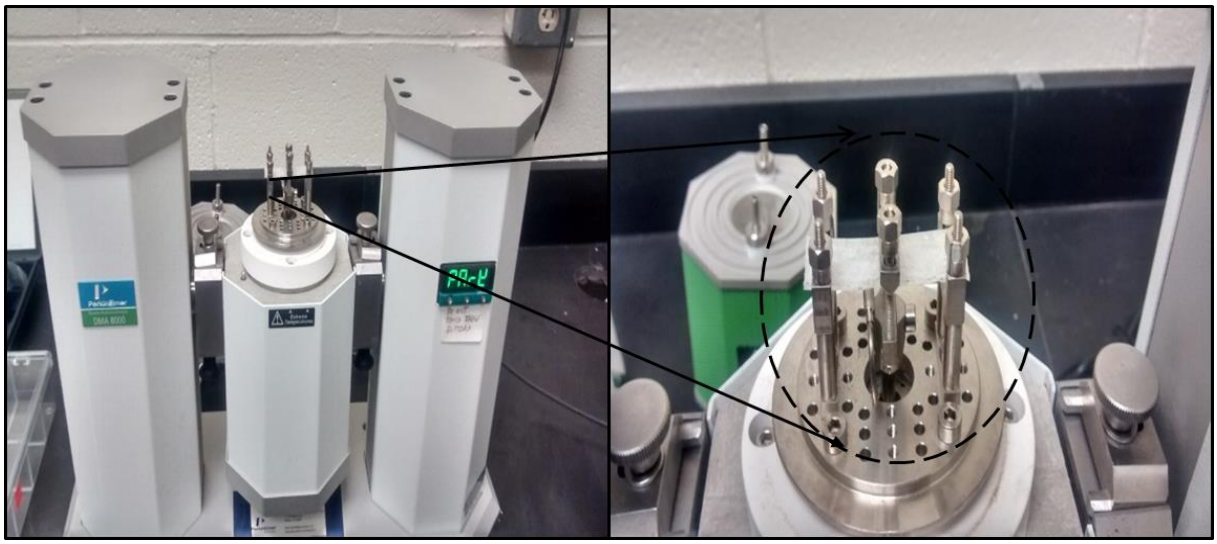

Figure 4.7: DMA Setup (Perkin Elmer DMA 8000)

Figure 4.8 shows the evolution of storage modulus and loss modulus of SMP with respect to temperature. Evidently, the polymer is quite stiff at room temperature and softens as the temperature is raised past T_g. The glass transition temperature range is observed to be from 45˚C to 65˚C which is evident from storage modulus and loss modulus function variations against temperature in the graphs presented in Figure 4.8a and Figure 4.8b. As the glass transition temperature is defined as the peak of the tan δ curve, by examining the tan δ curve shown in Figure 4.8c it was concluded that the T_g for the current polyurethane based SMP is approximately 62˚C.

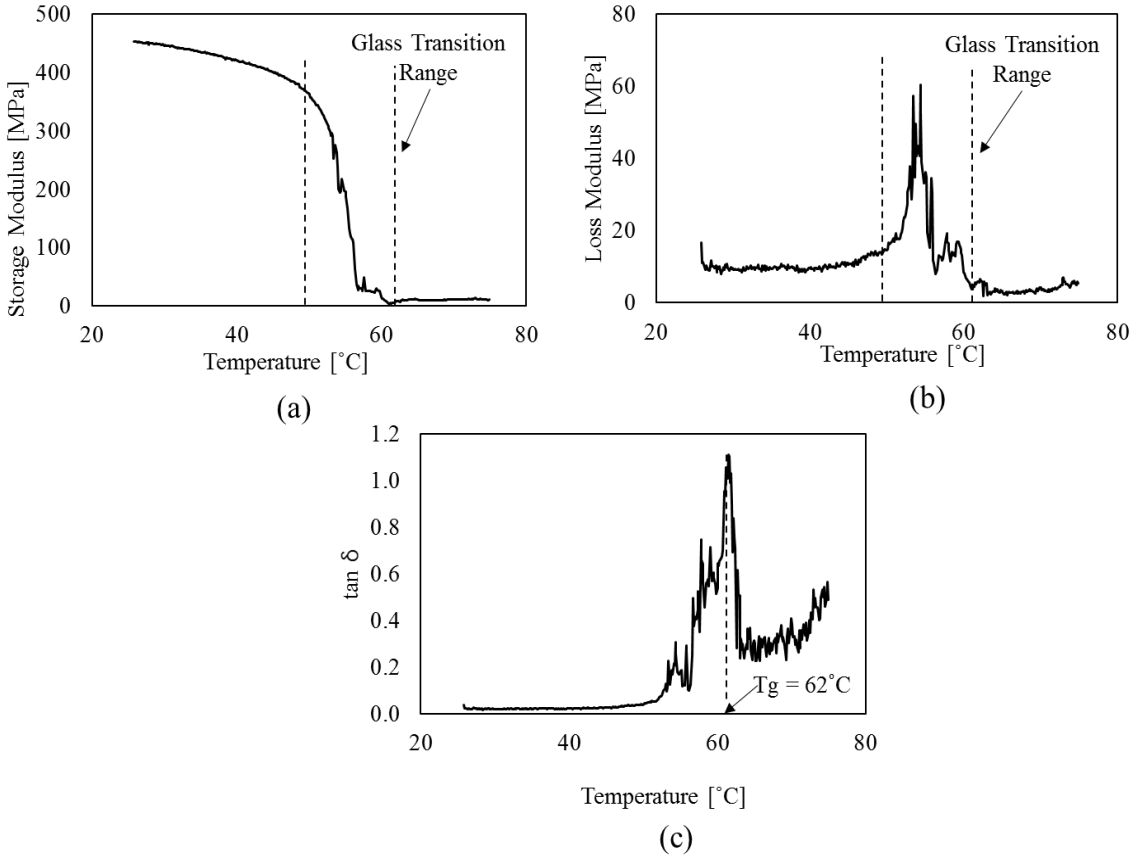

Figure 4.8: Dynamic mechanical analysis results: (a) storage modulus vs. temperature (b) loss modulus vs. temperature (c) tanδ vs. temperature

4.2 SHAPE MEMORY CHARACTERIZATION

Shape memory retention is the discerning quality of SMPs which differentiates them from other conventional polymers. Hence, it is of utmost importance to characterize SMPs for its shape retention and shape recovery characteristics. In general, universal testing machine is used to test the samples for stress-strain curves. Shape recovery and retention ratios are then calculated from those curves (Guo et al., 2015). These traditional tests are not very suitable for all SMP types. For this study, 'fold-deploy' shape memory tests (Liu et al., 2010) were performed to evaluate shape memory characteristics. The test essentially consists of three steps: firstly, the samples are heated above the transition

temperature using a heat gun. As the material flexes, it is bent about its central axis. The maximum bending angle is recorded at this point and hereafter named as $\theta_{max.}$ In the next step, the bending forces are held constant and the specimen is cooled below its transition temperature. The forces are then removed and the bending angle is recorded again at this stage and is termed as θ_{fixed}. For the third and final step, the specimen is heated in steps until the maximum shape recovery is observed. The bending angle is recorded at intervals of 20s and termed as θ_i. The shape recovery process for pure SMP is shown in Figure 4.9 below.

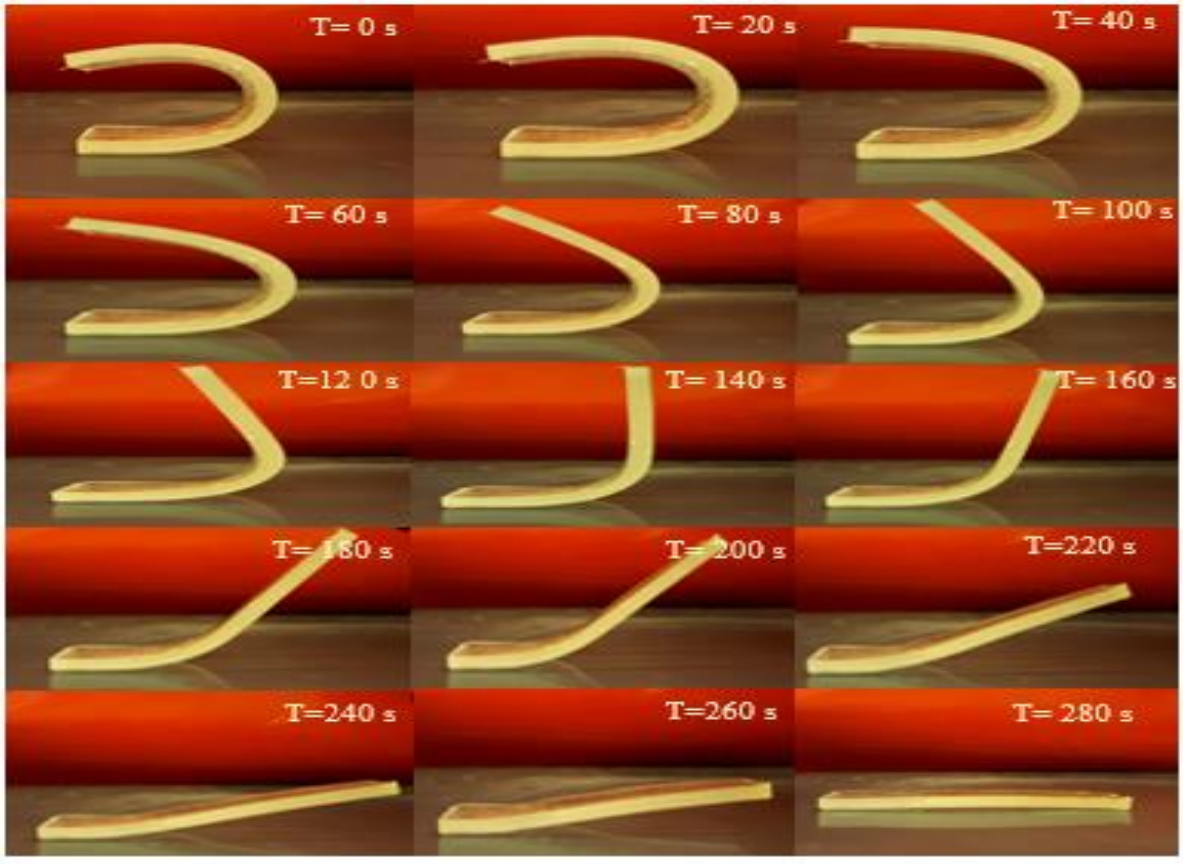

Figure 4.9: Shape recovery in pure SMP

The shape retention and recovery ratios are calculated as follows:

$$Shape\ Retention = \frac{\theta_{fixed}}{\theta_{max}} \times 100\ \% \quad (1)$$

$$Shape\ Recovery = \frac{\theta_{max} - \theta_i}{\theta_{max}} \times 100\ \% \quad (2)$$

It was found that the polyurethane based SMP used in the study has very high shape retention and shape recovery ratios. Shape retention as high as 99 % was observed for pure SMP samples. Also, in order to investigate the influence of heating temperature on shape recovery ratio, shape recovery performance (for the final step in fold-deploy test) was measured at varying heating temperatures (Figure 4.10). The heating temperatures considered are T_g (62 °C), T_g+15 (77 °C) and T_g+30 (92 °C). The bending angle in consideration is 180˚. It was observed that for the current SMP product, maximum shape recovery ratio which was 98% was independent of the heating temperature. However, increasing the heating temperature above T_g increased the rate of shape recovery significantly.

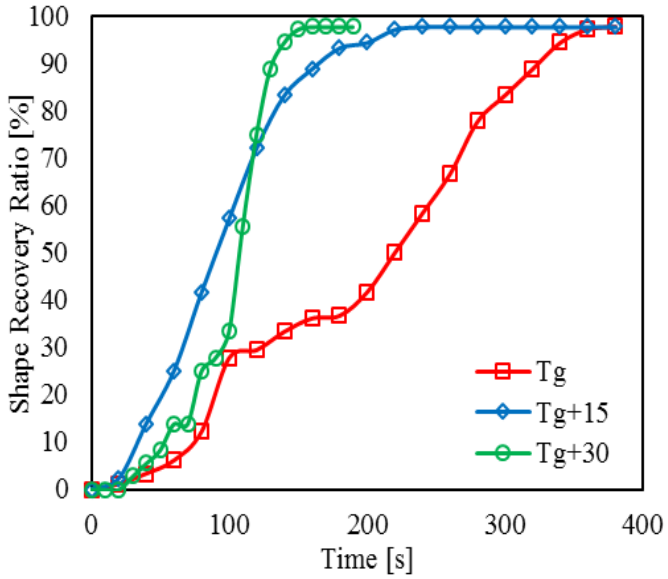

Figure 4.10: Effect of heating temperature on shape recovery ratio

CHAPTER 5: FINITE ELEMENT ANALYSIS

This chapter investigates the use of Finite Element Method (FEM) as a tool to model and analyze typical four-step shape memory cycle behavior of shape memory polymers from the phenomenological standpoint. The material properties developed in the process are applied in a full scale I-section beam model which incorporates a potential structural application for this material.

5.1 SHAPE MEMORY CYCLE CHARACTERIZATION

. For the simplest case, the shape memory characterization cycle for an SMP consists of four essential steps. The first step is heating the polymer above its transition temperature (T_{trans}), which renders the shape memory polymer quite flexible. The polymer at this stage can be transformed as desired to be fixed in any shape and form by the application of external force (or stress) at the temperature commonly termed as deformation temperature (T_d). For the second step, keeping the deformation constant (maintaining the level of force), the temperature is lowered at this point below the transition temperature and strains are allowed to fix rendering the shape to fixed in this particular temporary/intermediary shape. The strains at this level are termed as ε_{load}. The forces are removed at this point with the sample strain responding accordingly to a fixed strain ε and this marks the end of step 3 in the process. Importantly, deformation imposed onto the SMP at this point will be maintained even after the removal of the external force. This is simply due to the freezing of the molecular chain (i.e. reduction of chain mobility) that locks in the deformed chain conformation, or enables the storage of entropic energy in the system. For the fourth and final step, the permanent shape from this point can be recovered merely

by heating the polymer sample above its transition temperature, usually termed as T_r (recovery temperature) releasing the locked strains and allowing the polymer to go back to the least energy and equilibrium state. Here, T_{trans} is commonly equal to glass transition temperature, T_g for an amorphous SMP or melting temperature, T_m for a crystalline SMP, that can be measured using standard thermal analysis methods such as Differential Scanning Calorimetry (DSC) or Dynamic Mechanical Analysis (DMA) (Zhao et al., 2015). Figure 5.1 illustrates the typical shape memory cycle behavior experienced in SMPs.

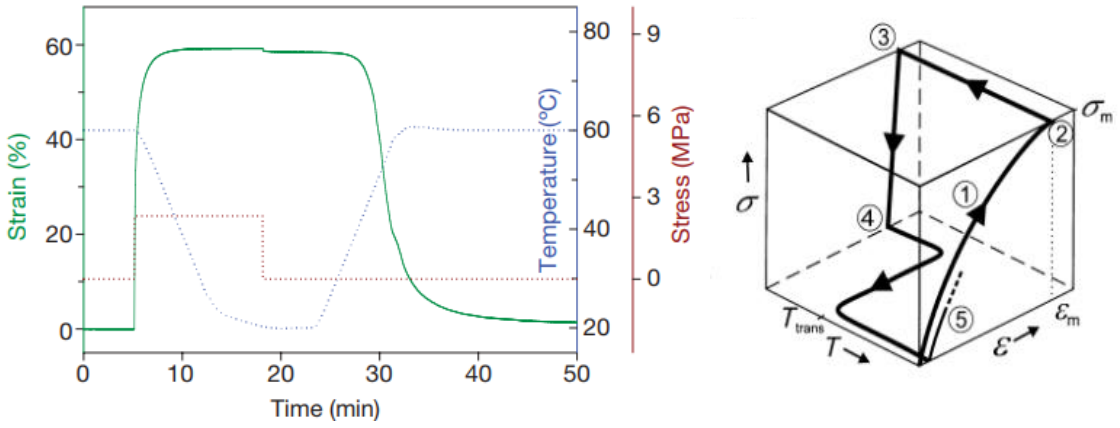

Figure 5.1: Quantitative dual-shape memory cycles: (a) 2D diagram (Xie, 2010) (b) 3D diagram (Lendlein & Kelch, 2002)

There have been several attempts to develop constitutive models for characterizing shape memory polymer behavior, but the most have focused on small deformation range, with nominal strains less than 10% in compression and tension (Souri, 2014). Most earlier models were based on simple spring-dashpot systems to capture the behavior of SMPs for small deformations (Tobushi et al., 1998), but were later modified to include nonlinear elastic terms, thermal expansion and viscosity to be better able to study viscoelasticity of

SMP for small deformations (Tobushi et al., 2001). However, a clear and more rational understanding of the behavior came from the phase understanding that SMP encounters during the shape memory effect, based on the model developed by Barot and Rao (2006). Subroutines based on this model have been developed by various researchers for different commercial programs, for instance, one such subroutine was developed for glassy shape memory polymers by Khanolkar et al. (2010). Liu et al. (2006) also proposed a model that defines the strains as fractions of elastic, thermal and stored components. The stored strain component is attributed to the deformations in the frozen phase. On heating the sample, the stored strain components recover, essentially transporting the material back to its permanent shape. Based on the principles developed by Liu et al. (2006) , Chen and Lagoudas (2008) developed a model that has the capability to support even large deformations. It is based on the premise that SMP is composed of individual particles as depicted in Figure 5.2. It is further assumed that individual material particles transform from the frozen (glass) phase to the active (rubber) phase at different temperature ranges and vice-versa, until the entire material has transformed into a single phase. The model was formulated in terms of average deformation gradient with a suitable integral technique used over the whole volume to calculate the average deformation gradient. The deformation in this model is assumed to be constant throughout.

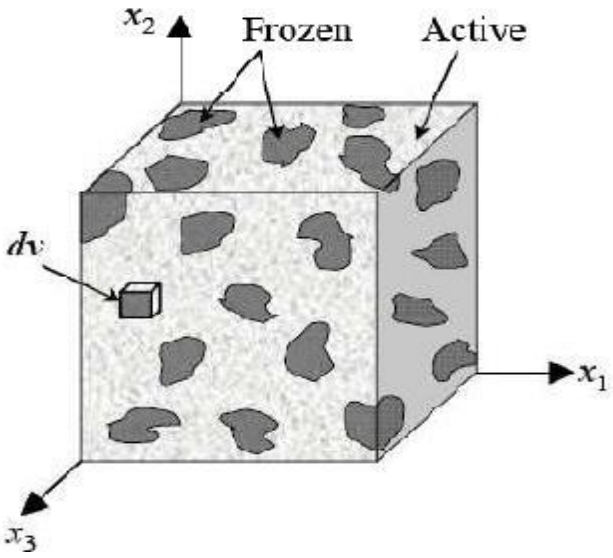

Figure 5.2: SMP composed of active and frozen phases in the model proposed by (Volk et al., 2010)

However, for the current study, to determine the shape memory cycle characteristics on a phenomenological level, a simplistic model based on Souri (2014) was developed, with the SMP deformed only in compression. Temperature dependent elastic and plastic property definitions are used to suitably define the material properties. The geometry consisted of a simple cylindrical shape with the diameter of 6.35 mm (0.25 in) and length of 76.2 mm (3 in) as shown in Figure 5.3.

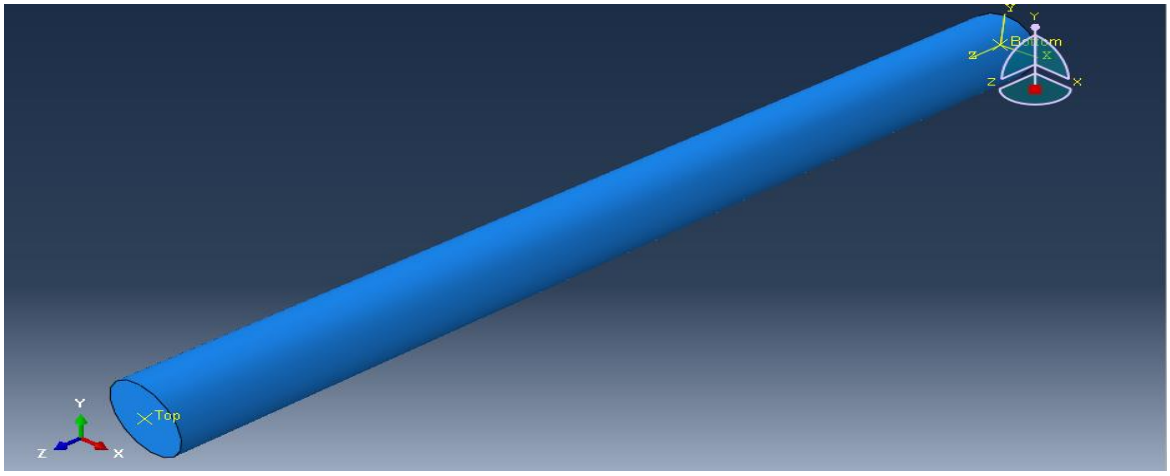

Figure 5.3: Cylindrical geometry for SMP behavior

Material properties based on the Souri (2014) study were provided, which consisted of temperature dependent elastic and plastic property definitions to simulate the shape memory behavior when the material undergoes transition from rigid to rubbery region and vice versa. Table 5.1 enlists the elastic material properties assigned to the material and Table 5.2 enlists plastic property definitions used for modelling in ABAQUS.

Table 5.1: Elastic Material Properties

Young's Modulus (MPa)	**Poisson's Ratio**	**Temperature (K)**
1300	0.3	280
900	0.3	298
400	0.4	308
300	0.4	318
200	0.45	328
100	0.45	373

Table 5.2: Plastic Material Properties

Yield Stress (MPa)	**Plastic Strain (%)**
70	0
45	5
50	18
70	50

As is also evident from the Figure 5.4 that the elastic modulus changes gradually as the material goes from rigid region to rubber region, going past the transition temperature, T_g (316K or 43˚C) defined for the material.

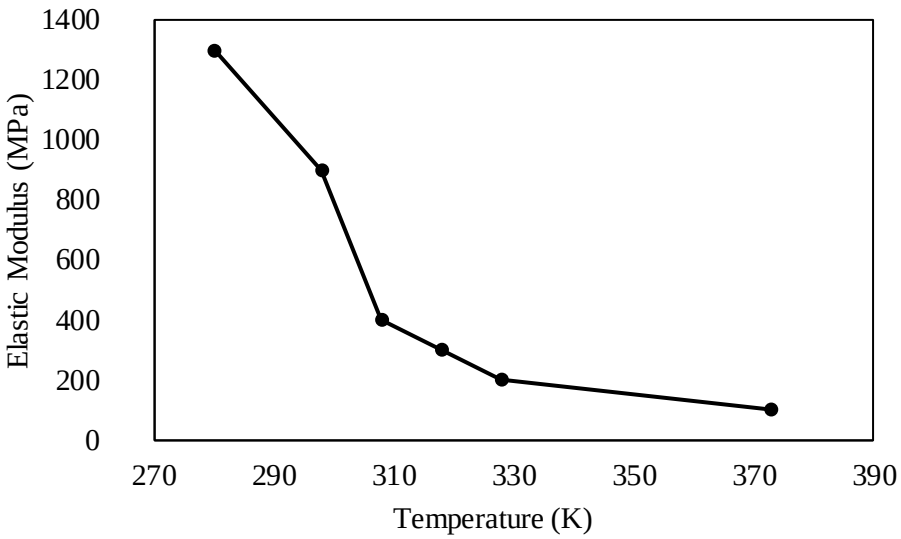

Figure 5.4: Elastic Modulus v/s Temperature

Table 5.3 highlights the thermal coefficient variation with respect to the temperature used for the current SMP material.

Table 5.3: Thermal Expansion Coefficients

Coefficient of Thermal Expansion (1/K)	Temperature (K)
2.30E-06	280
2.30E-06	298
2.30E-06	308
1.17E-05	318
1.17E-05	328
1.17E-05	373

The coefficient of thermal expansion variation used for the SMP material is also defined graphically in Figure 5.5.

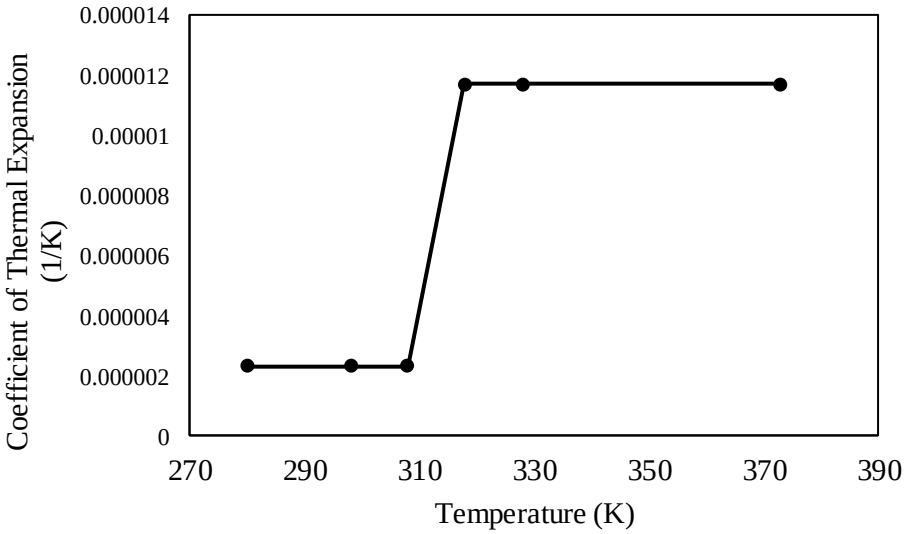

Figure 5.5: Coefficient of thermal expansion v/s temperature

To prevent any rigid-body motion of the sample in consideration, the bottom surface was coupled to a reference point defined on its surface and its kinematic motion was restricted in all three major directions, along with any rotation. The load in the force controlled mode or the displacement in the displacement controlled mode was applied to a reference node which was coupled to the top surface as defined in Figure 5.6.

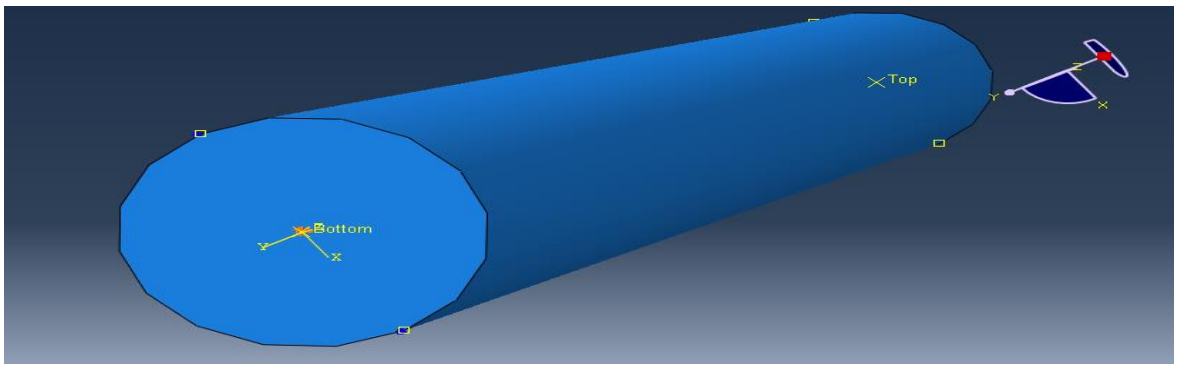

Figure 5.6: Node Constraints

The mesh module in ABAQUS can be used to generate the meshing for different components of the finite element module (Dassault Systémes, 2014). Linear hexahedral

elements of the type C3D8R were used for the current study. Initially, default mesh size was used, which was modified further to get higher accuracy in results. Figure 5.7 shows the final meshed assembly.

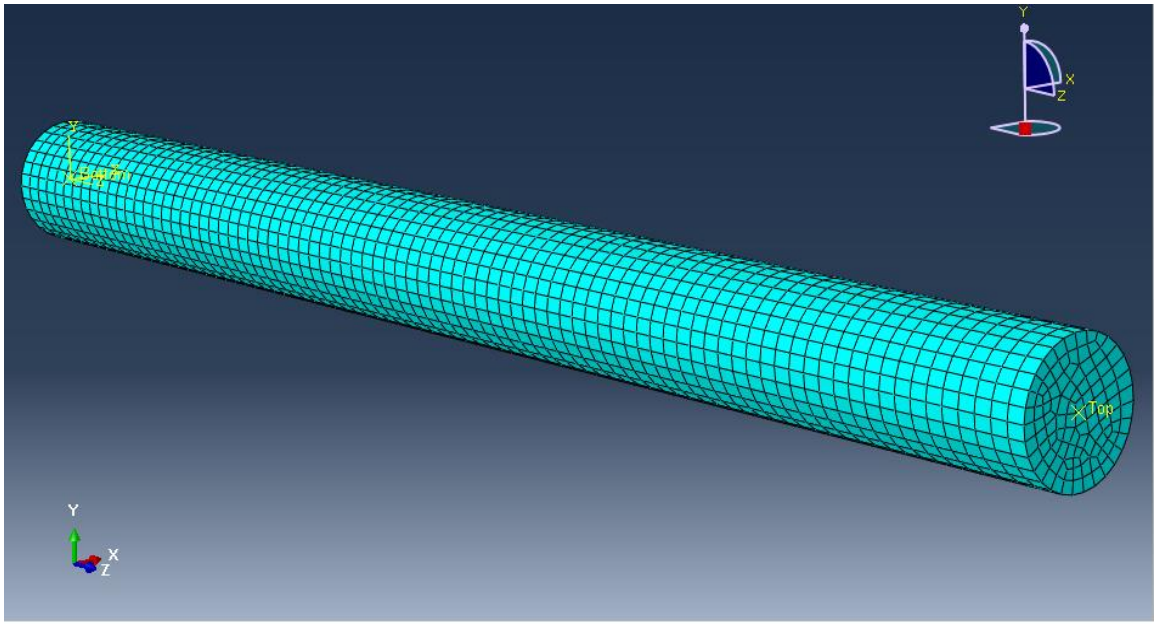

Figure 5.7: Final meshed assembly

The step module in the ABAQUS software can be used to generate different steps for the sequence to be followed in the loading analysis of the model in consideration. Different types of analysis like static, dynamic, cyclic loading analysis can be performed using the software. Initially, the steps were defined in such a manner that the process was entirely load controlled with the following step definition in order:

- Initial Step: All the initial conditions were set. The temperature was set to 363 K, which is above the glass transition temperature, and load at zero.
- First Step: The temperature was kept at 363 K which is above the defined transition temperature for this material so as to keep it in the rubbery region and a compressive load of 1500 N (approximately 75 MPa) was applied to the top surface.

- Second Step: While the load was kept constant, the temperature decreased with a constant rate to 263K, which is lower than the T_g, which renders it quite rigid while the stress is kept constant.
- Third Step: The load was removed and the temperature was kept constant. Thus, the elastic deformation was released and the sample remained deformed as per the definition of plastic strains applied.
- Fourth Step: This is the recovery step, the temperature was increased with a constant rate up to 363 K which is above T_g, the glass transition temperature at which the sample will recover back to its original shape.

The Figure 5.8 shows the temperature protocol for the loading scenario described in the step definition above.

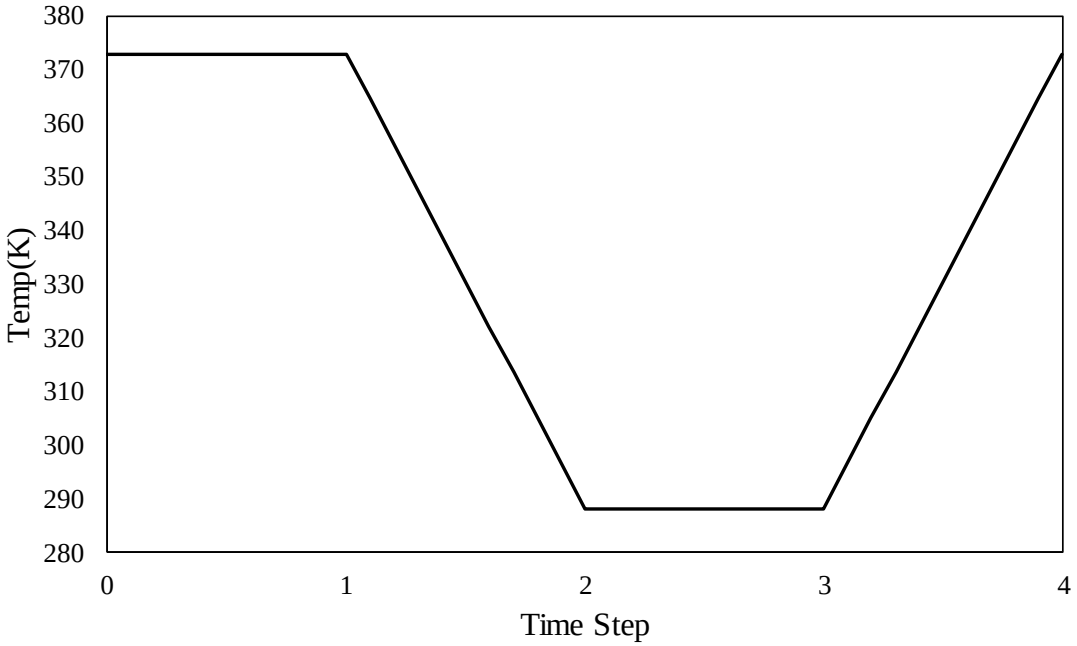

Figure 5.8: Temperature Profile for the shape memory cycle

Figure 5.9 shows the strain variation obtained from the shape memory cycle with the step defintions defined above. As evident from Figure 5.9, the material reaches a strain value (0.66%) as the sample is loaded. The elastic component of the stored strain is released in the third step with the sample bieng unloaded. With the final heating , the material comes back to the original shape with zero strains.

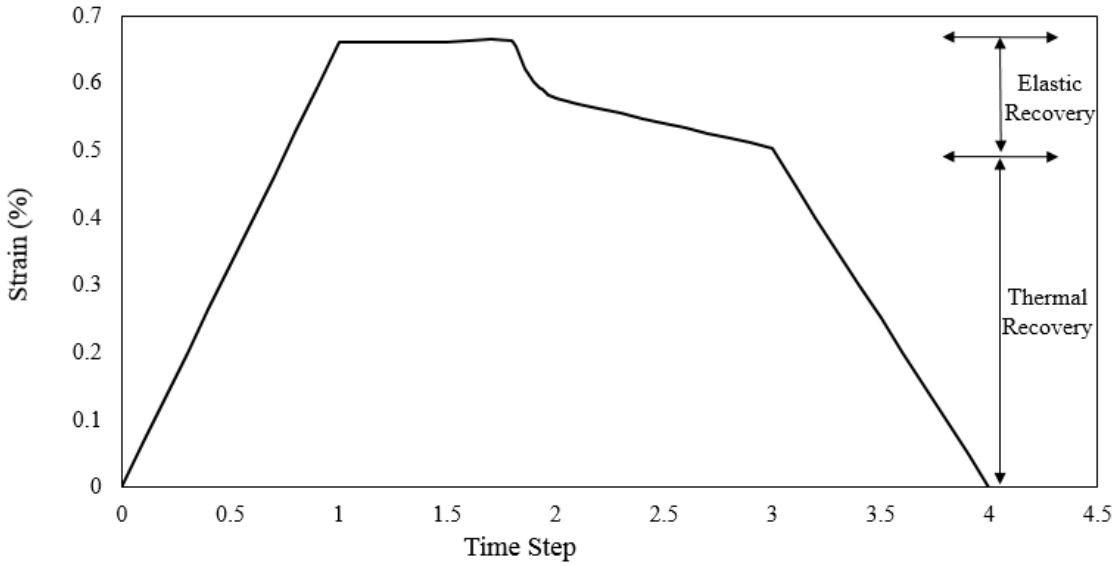

Figure 5.9: Elastic strain v/s time step

Figure 5.10 shows the variation of stress consistent with the step definition defined above. The stress reaches a plateau (50MPa) for the first step when the specimen is deformed in compression. It remains at this constant value for the cooling step when the temperature is lowered and thereby maintains the deformation level. The stress reaches a zero magnitude as the applied force is removed in the third step of shape memory cycle. A portion of stored strain component is recovered in this process as shown in Figure 5.9.Finally in the last step, as the temperature is raised to 363K, past the glass transition

temperature,T_g , the stored strains are recoverd and the material recovers its permanent shape , attaining a state of least internal energy.

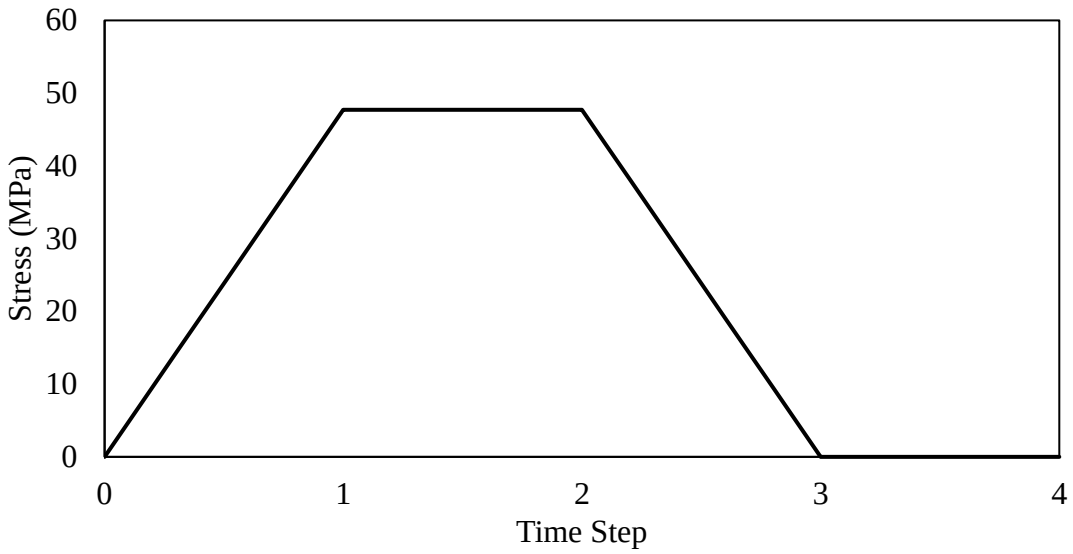

Figure 5.10: Stress v/s time step

Since the post-peak behavior is not obtained for the force controlled deformation of the SMP sample, in the later stages, the deformation was applied in the deformation controlled mode, while the step definitions and other loading conditions were kept the same. This whole cycle including the aforementioned four steps could be seen in the Figure 5.11,which shows the displacement magnitude along the major axis of the member.

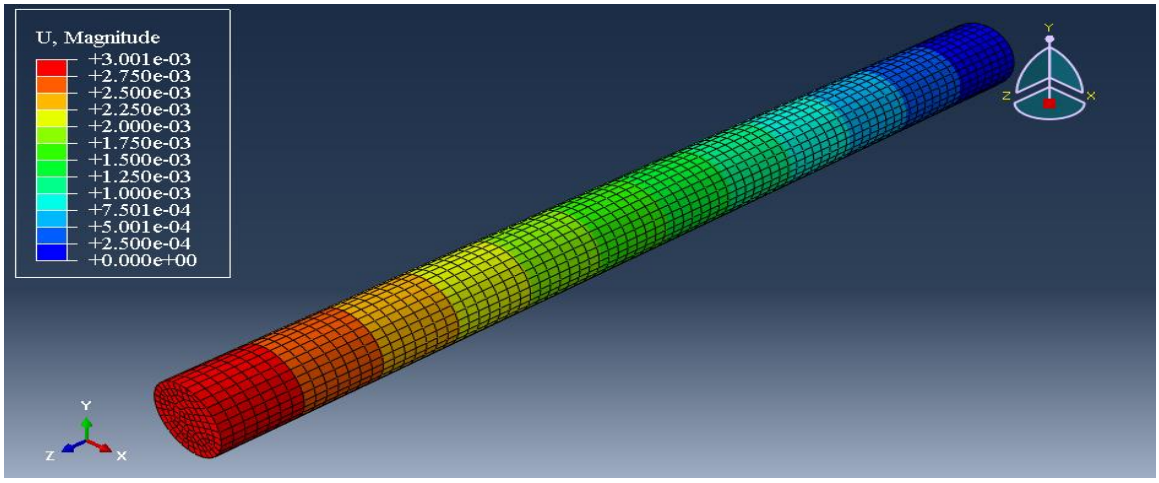

(a) Loading Step

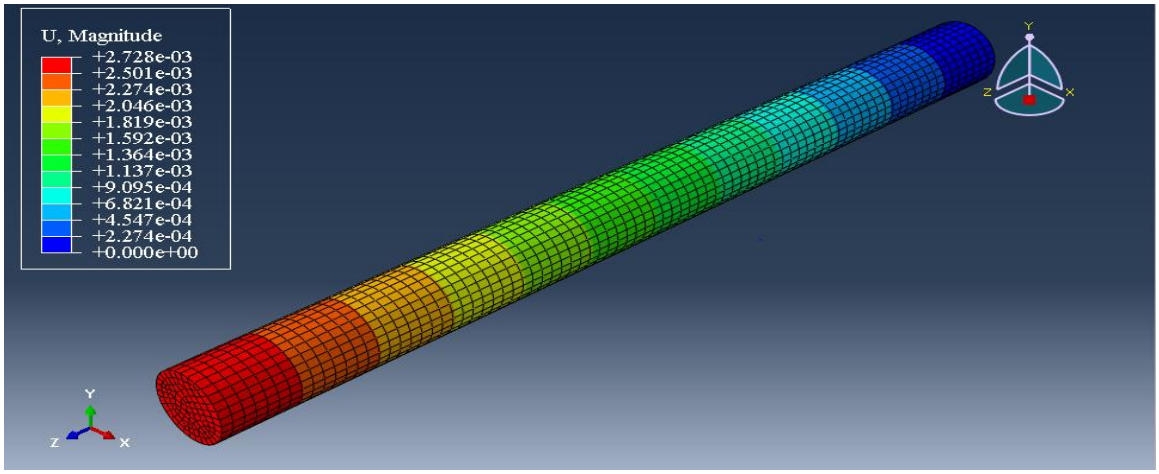

(b) Cooling Step

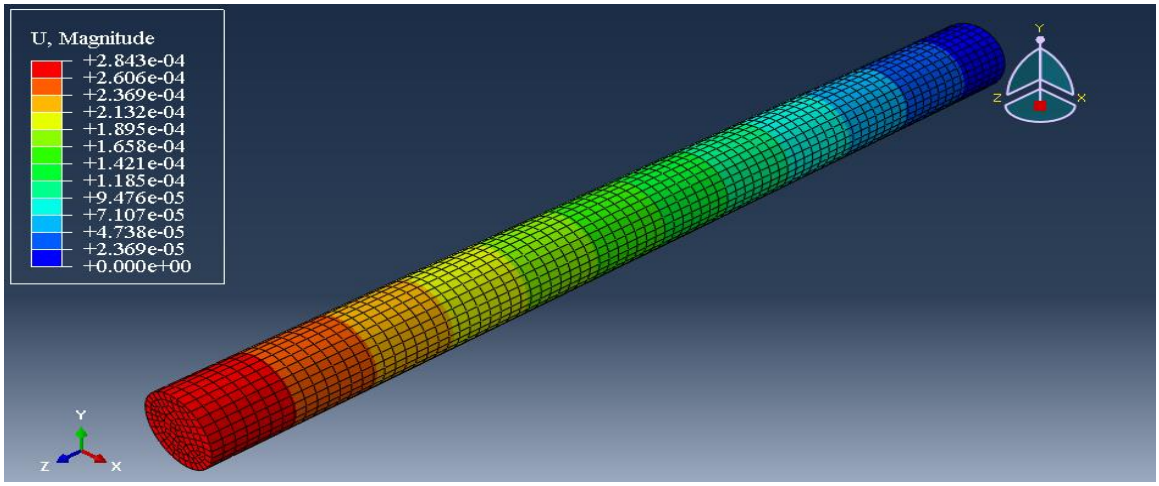

(c) Unloading Step

Figure 5.11: Steps in SMP characterization cycle

Figure 5.11 (cont)

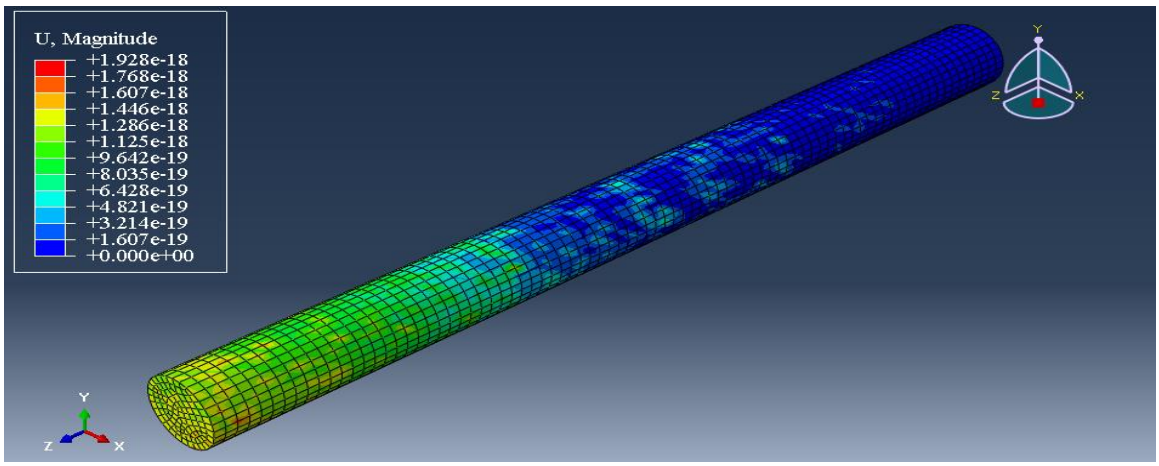

(d) Recovery Step

The Figure 5.12 shows the graphical representation of the shape memory cycle on a 3D-plot.

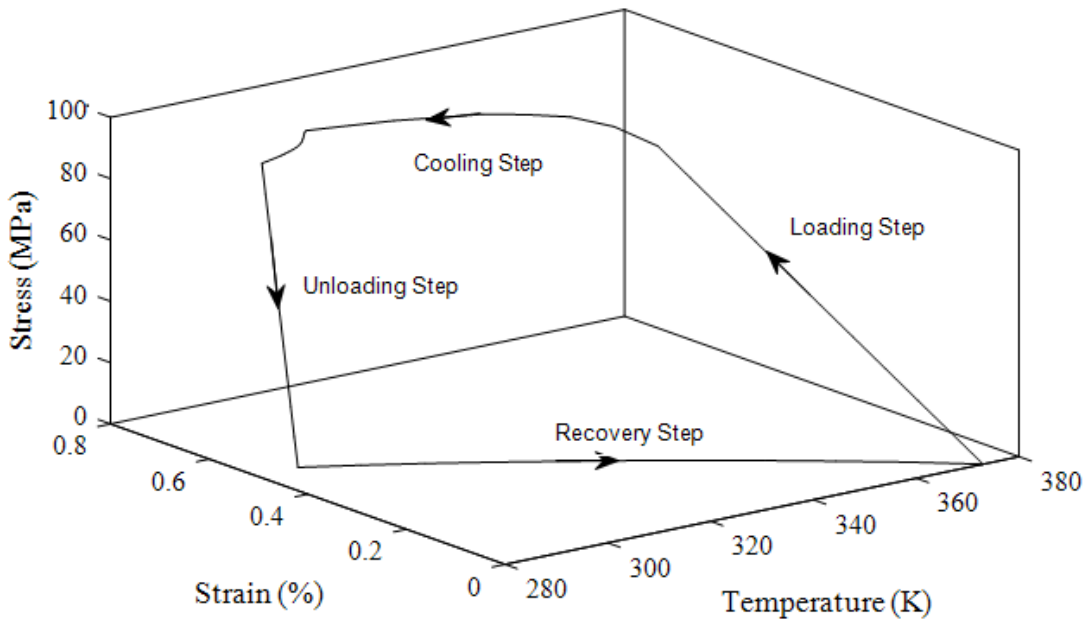

Figure 5.12: 3D plot for SMP cycle

The graph in Figure 5.12 clearly outlines the four different steps used to characterize the shape memory behavior of the cycle and characterize the material. The little drop in stress after the cooling step could be attributed to the elastic relaxation in the fixing step (as the shape fixidity is not 100 % for all the cases). This could be attributed to the definition of temperature dependent material properties assigned for this material. More advanced material models based on the kinematics of frozen fraction and average deformation gradients as described previously would not show this effect.

5.2 SMP POTENTIAL STRUCTURAL APPLICATION

The proposed concept aims to use SMPs in creating structural components for various applications in building and bridge industry. As they can be molded to any desired temporary shape after the characteristic shape fixidity step in the shape memory cycle, they will be easy to store, pack and transport on site, with enormous cost savings. One such potential application cab be in developing structural components with foldable flanges. Flanges developed from shape memory resin reinforced with fibers will fold and unfold themselves as per the shape memory characteristics programmed into them during the manufacturing process. Figure 5.13 illustrates this simple approach of loading and unloading of an I-section with shape memory components.

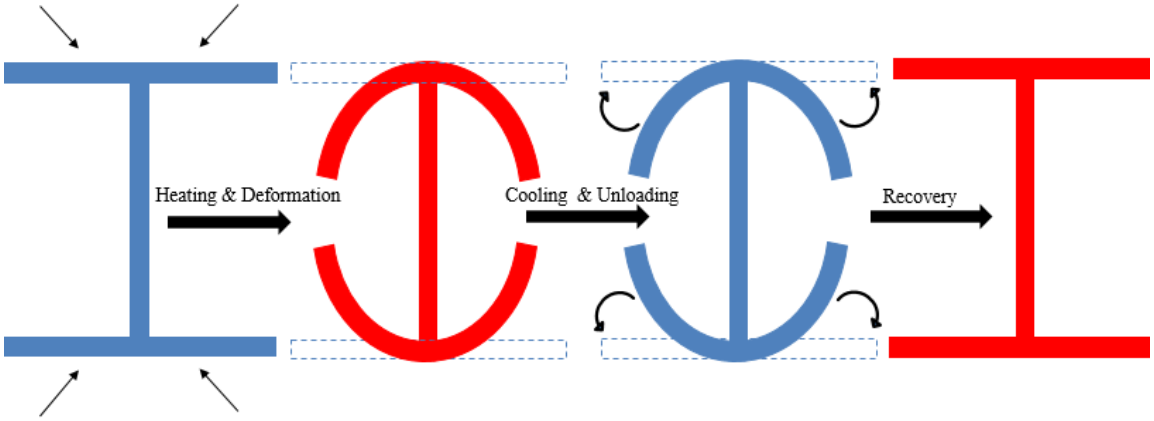

Figure 5.13: Potential shape memory application in I-section

To achieve the desired advantages of SMP structural components, SMP composite components can first be manufactured on a plant in close proximity to the construction project site. With the application of heat, it will tend to soften, making it ideal for deformation in a temporary compressed shape. The folded components will then be shipped on site and off loaded on the supporting components. The bottom flanges will unfurl themselves upon application of heat. Rest of the folds can then later be unfolded upon the application of heat (or passage of electric current). To validate the concept, FEM model was developed that ensues this concept with the dimensions and section properties shown in Figure 5.14

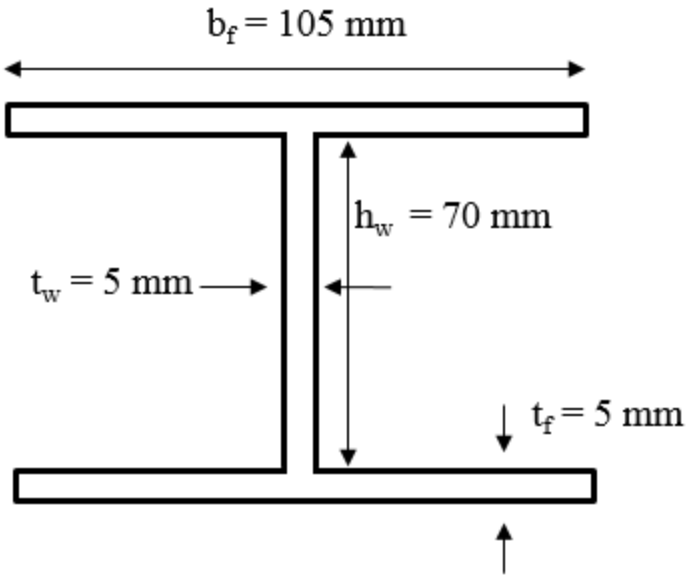

Figure 5.14: Cross-sectional dimensions for the beam

Figure 5.15 shows the model of the geometry developed in ABAQUS with the length of the beam specified to be 300mm.

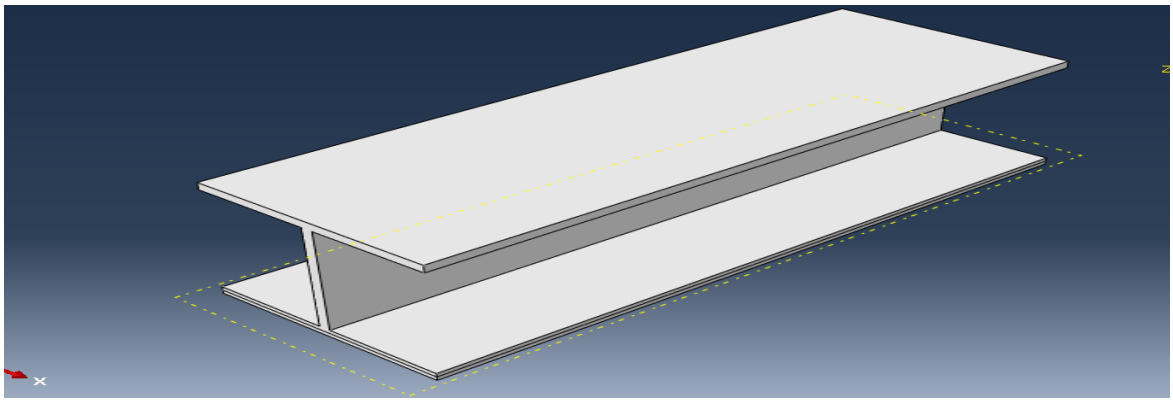

Figure 5.15: Geometry for the beam model

The model generated was meshed using linear heahedral elements for both the flanges and the beam. Finer mesh was used for the foldable bottom flange of the beam to improve the accuracy of the results. The Figure 5.16 shows the meshed model with linear hexahedral elements. The mesh was refined to improve the accuracy of results.

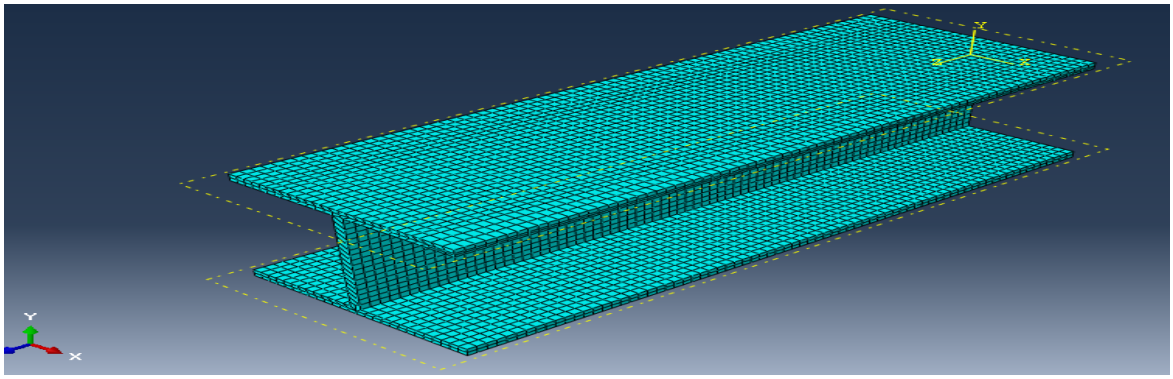

Figure 5.16: Meshed assembly

For the boundary conditions , the top flange and web were given fixed boundary conditions completely restricting any motion in all major directions which is depicted in the Figure 5.17. The bottom flange is allowed to displace and rotate as per the loading conditions.

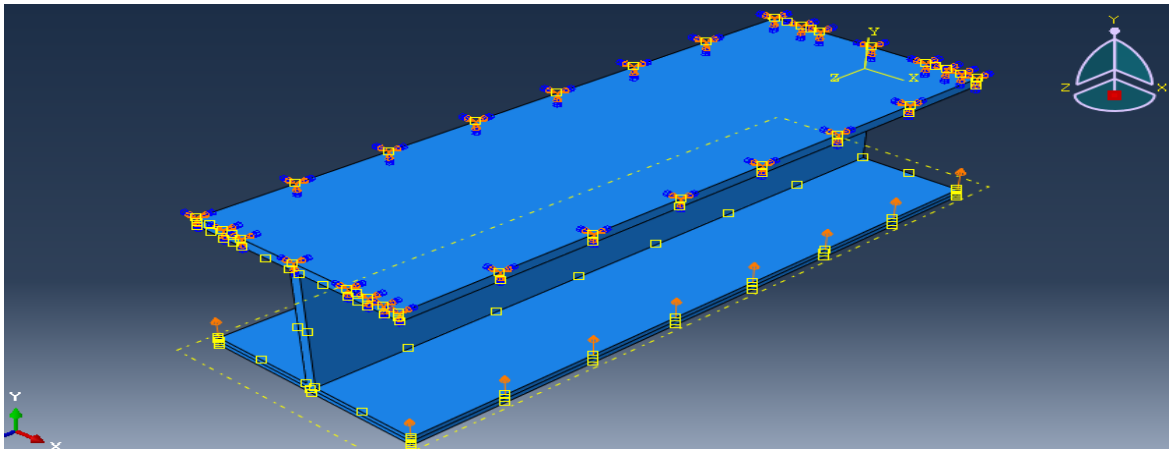

Figure 5.17: Loading and boundary conditions

The previously developed material model for SMP was successfully applied to the bottom flange to give it shape memory characteristics. The displacements were applied

symmetrically at the two top end edges of the bottom flange. Figure 5.18 shows the magnitude of displacements and effectively the shape memory behavior exhibited by the flanges, which could potentially be used for developing different structural components as described above.

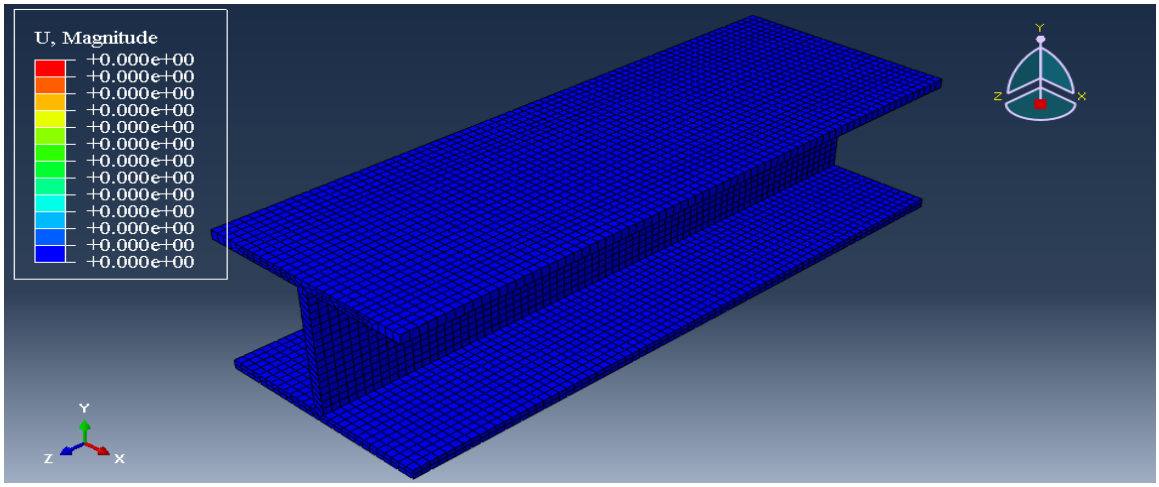

(a) Reference Configuration

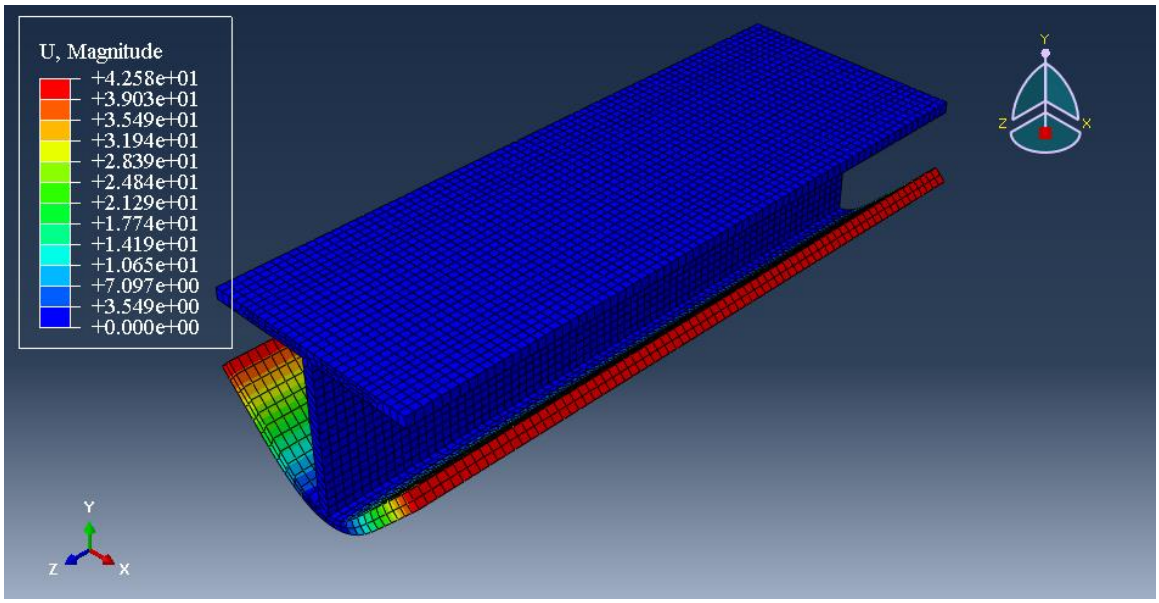

(b) Loading Configuration

Figure 5.18: Shape memory behavior in beam flange

Figure 5.18 (cont)

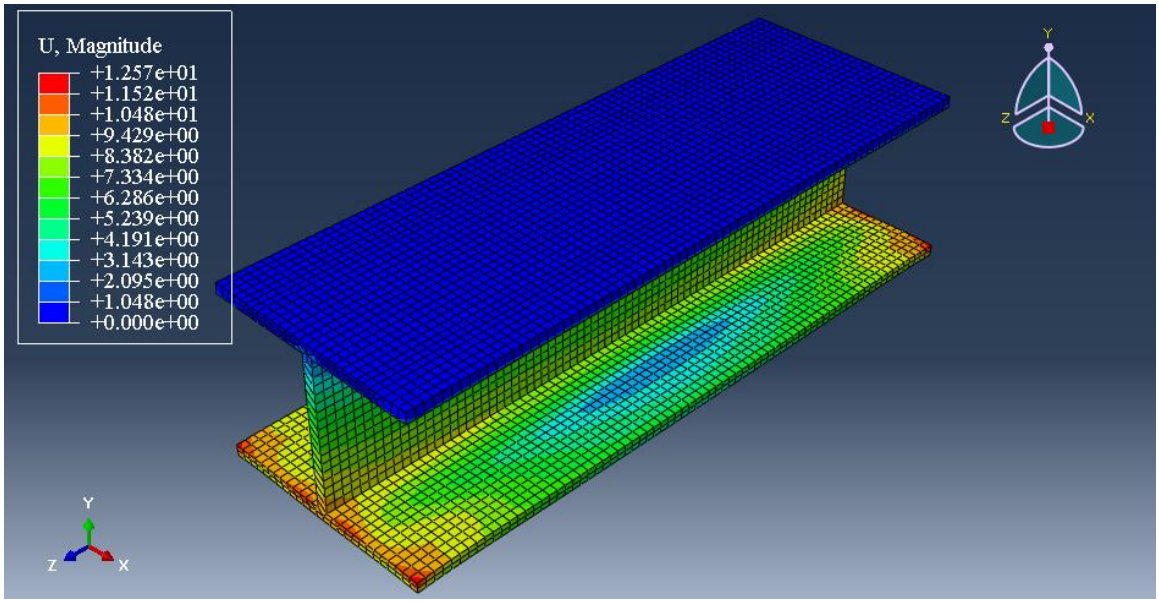

(c) Recovery

However, it was observed that pure SMPs, severely lack many properties that make them unsuitable for various functions, specifically that require high mechanical properties, like high stiffness and strength. This was observed as well with low stress values obtained from simulations (~20 MPa). In accordance, next chapter deals with characterizing SMP and its carbon fiber fabric reinforced composite (SMPC) to study in greater detail the improvement in mechanical characteristics via three important parameters namely Young's Modulus, Ultimate Strength and Ultimate Strain.

CHAPTER 6: MECHANICAL TESTING

In order to mechanically characterize the pure SMP and investigate the impact of adding carbon fiber fabric on the strength, ultimate strain and Young's Modulus of the so formed SMP composite (SMPC), static tensile tests were performed.

6.1 TEST SETUP

The quasi-static tests were performed in a displacement controlled mode with a constant crosshead speed of 2 mm/min. A ±20kN load cell was used with the testing machine. An extensometer with a gauge length of 25.4 mm was used at approximately mid height of the coupon specimen to measure axial strains. Figure 6.1 shows the universal tensile testing machine setup for the testing of coupons. As illustrated in Figure 6.1, the used specimens had a rectangular shape and were 158.75 mm long, 25.4 mm wide and 12.7 mm thick with a gage length of 44.45 mm. Chamfered tabs with bevel angle of 7-8° were used at both ends of the specimen.

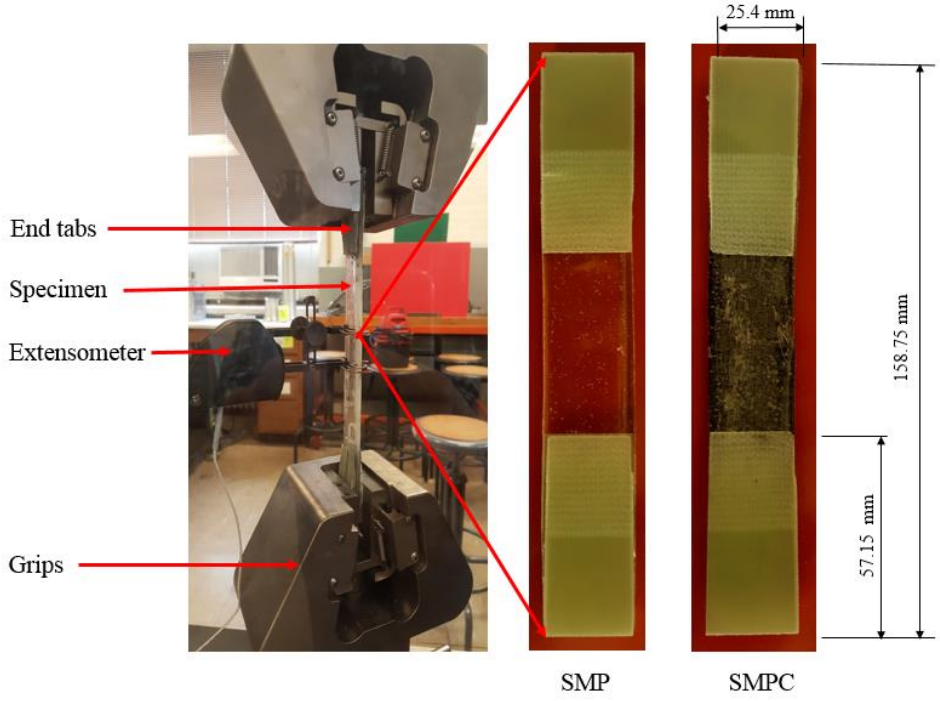

Figure 6.1: Tensile testing setup and specimens

In the static tensile tests, engineering stress and strain properties were used to determine the characteristics of SMP and SMPC. Stress-strain plots were generated for pure SMP and SMPC and compared for primarily three parameters, tensile strain at failure, tensile strength and Young's modulus in the linear elastic region. Figure 6.2 shows a sample stress-strain plot for the SMP and SMPC. The carbon fabric used in the SMPC was aligned in the longitudinal direction of the specimen. In designing the SMPC specimens, the Young's modulus of the composite (E_c) was represented as:

$$E_c = E_m V_m + E_f V_f \tag{3}$$

where, E_m and E_f are the Young's modulus for matrix and fiber, respectively, and V_m and V_f are the volume fiber fraction of matrix and carbon fiber, respectively. The volume fraction of the carbon fiber for the samples tested was approximately 2%.

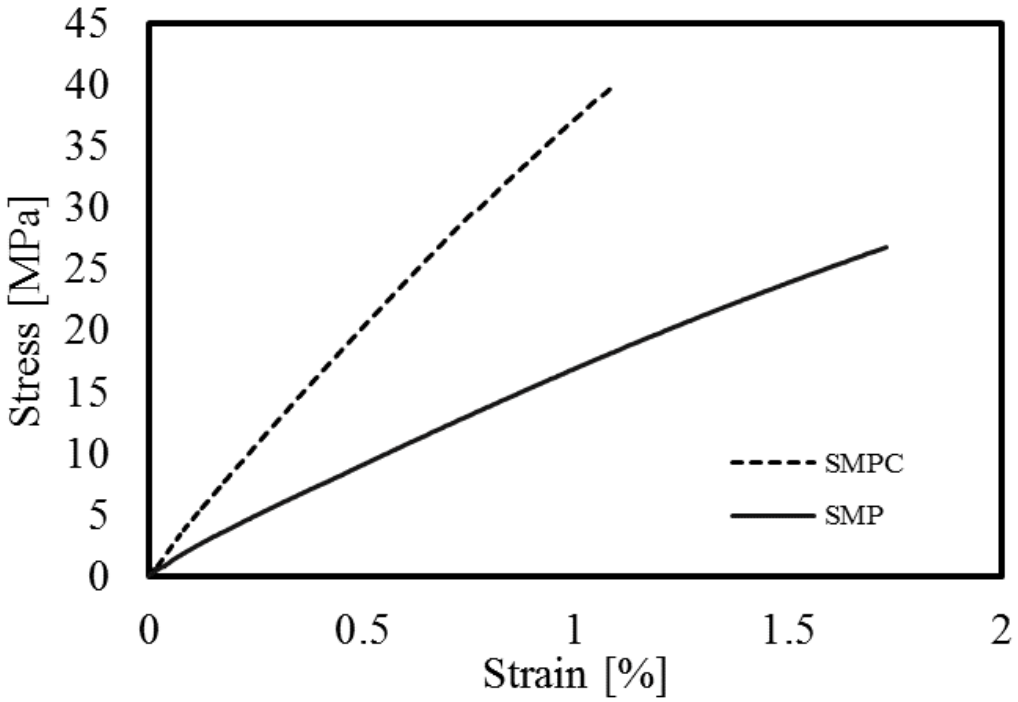

Figure 6.2: Stress-strain for Pure SMP and SMPC

From the bar graph in Figure 6.3, it can be observed that with the addition of carbon fibers, the stiffness for SMPC increased considerably from its pure SMP counterpart.

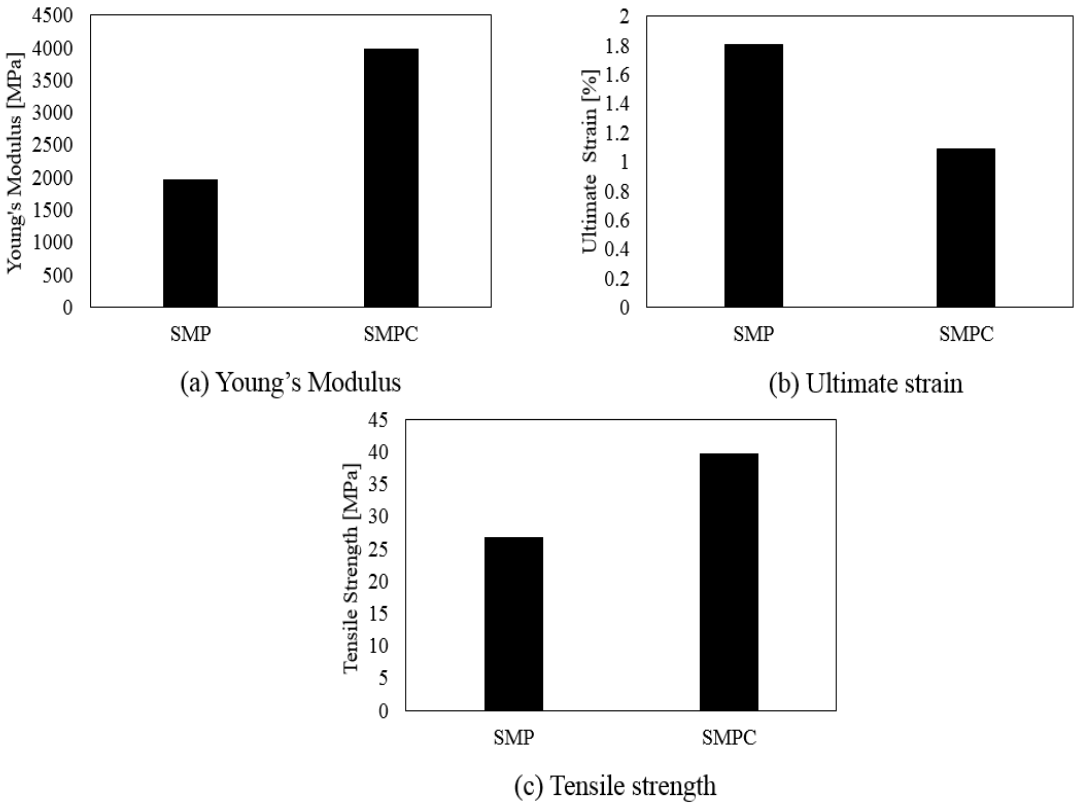

Figure 6.3: Tensile testing results for SMP and SMPC

The modulus for the SMPC specimen was observed to be 3980.56 MPa, whereas for the SMP it was close to 1977.60 MPa. Stiffness nearly doubled for SMPC specimen, leading to a rise of approximately 100%, as was expected from theoretical calculations based on the rule of mixture for composites as described in Equation 3.

Fracture stress and strain values were also observed from the longitudinal stress-strain curves of the SMP and SMPC. The comparison is elaborated via the bar graph in Figure 6.3. Maximum strain observed for the pure SMP samples was close to 1.88 % while for SMPC it was observed to be 1.09 %. This approximately 40% reduction in the ultimate strain value can be attributed to the limiting strain capacity for carbon fibers used as

reinforcement in the SMP matrix. The fracture stress increased by approximately 50 % for the SMPC compared to SMP.

6.2 EFFECT OF DEFORMATION

The developed SMP and its composite (SMPC) have the potential to be used in various structural applications. It is thus of utmost importance that the mechanical properties of the material does not degrade considerably after substantial usage. To account for this, the mechanical properties of SMP and SMPC were examined prior to and after undergoing extreme cycles of deformation and shape recovery. As depicted in Figure 6.4, each cycle consisted of first heating the specimen above T_g to render it flexible. Next, the specimen was subjected to excessive deformation in the form of bending (with a maximum bending angle of 180˚), followed by cooling to lock the strains. Finally, the specimen was heated again past the glass transition temperature to recover back its original shape.

Figure 6.4: SMP specimen undergoing shape memory cycle

Three cases were considered for this study, namely, no deformation as-built case, one shape memory cycle case, and four shape memory cycles case. The parameters of

interest were elastic modulus, strength and ultimate strain. A summary of the results is shown in Figure 6.5.

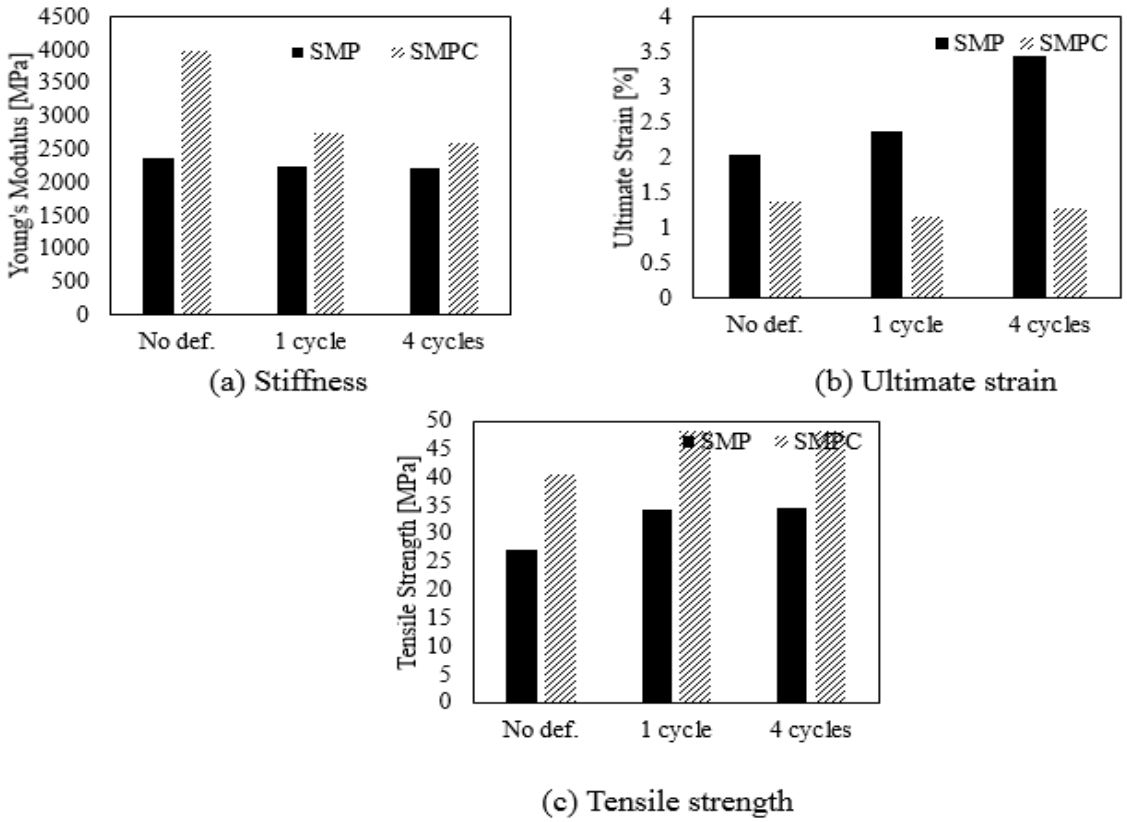

Figure 6.5: Effect of 180˚ bending shape memory cycles on mechanical properties of SMP and SMPC

As shown in Figure 6.5 (a), the stiffness decreases considerably as the sample undergoes 180° shape memory bending cycles, for both SMPC and SMP specimens. Notably, the major drop in stiffness is observed after the first shape memory cycle and the drop after subsequent cycles is very small. For example, in the case of SMPC samples, as the sample undergoes 1 shape memory cycle, the elastic modulus is reduced by 45 % and there is a minor reduction of 5% in stiffness when the sample undergoes 4 shape memory cycles. Also, for all three cases, Young's modulus increased for the case of SMPC in

comparison to pure SMP. However, as the specimen underwent four shape memory cycles, the percentage increase in modulus for SMPC compared to SMP dropped down to merely 18% as opposed to the case when it didn't undergo any shape memory cycles, where the rise was approximately 100%. This may be due to the considerable rearrangement of molecular chains inside the SMP matrix leading to slip between the carbon fiber fabric and the SMP matrix and reduced interlocking of the fiber with the matrix.

On analysing ultimate strain of the samples (Figure 6.5(b)), it was observed that the strain of SMP increased with increasing the number of cycles by as much as 69% for the 4-cycle case when compared with as built case. This increase may be attributed to the Brownian motion and changes in molecular arrangement in the SMP matrix, which lead the specimen to become excessively flexible after going a number of characteristic shape memory cycles. On the other hand, the number of cycles seem to have opposite impact on the SMPC, where a decrease of 16 % was noted in the ultimate strain when SMPC was subjected to one cycle only, when compared with no deformation as-built case. Subjecting the SMPC to more cycles didn't seem to have significant additional impact on the ultimate strain as it only resulted in a decrease of 1.15 % compared to the one cycle case. This observation with major deviation after 1 cycle and no considerable change after subsequent cycles, in ultimate strain holds true even for stiffness as evident in (Figure 6.5(a)) and even for strength (Figure 6.5(c)) as described further.

Analysing the tensile strength of SMP and SMPC (Figure 6.5 (c)) revealed that, for the as-built case, the tensile strength of SMPC is higher than that of SMP by approximately 48 %. This difference is analogous to the results previously obtained (see Figure 6.3(c)). Also, on average, this rise in stiffness comparing as-built SMPC and SMP specimens, is

maintained as the samples undergo one characteristic shape memory cycle. The rise between SMP and SMPC is not as significant (39 % rise) as the sample undergoes 4 shape memory cycles. This may be due to flexing of samples with large number of cycles. In addition, comparing only SMP samples, the tensile strength rises by 25 % as the sample undergoes one shape memory cycle and the rise is approximately 1-2 % as it further undergoes 4 characteristic shape memory cycles. Analogous to this, comparing only SMPC specimens, the tensile strength first rises by approximately 18 % for one cycle and drops to 1-2 % as it further experiences more shape memory cycles. The reason for this behavior can be attributed to the fact that the deformation and failure govern the first cycle, whereas training and memorizing effect of the shape memory polymer governs the subsequent cycles, causing it to stabilize after a while.

6.3 EFFECT OF BENDING ANGLE

A parametric study was conducted with the SMP and SMPC specimens to study the effect of deformation angle on the mechanical properties of the polymer in pure and composite forms. Three different bending angles, namely 45˚, 90˚, and 135˚ were considered in the study. Initially, specimens (both SMP and SMPC) were heated above their glass transition temperature and deformed to required angles. Subsequently when the specimens were cooled down the applied bending force was removed and strains were kept fixed. The state was maintained for a duration of 1 hr and then the samples were heated again past their transition points to recover back the locked deformation. Figure 6.6 shows specimens under various levels of deformation.

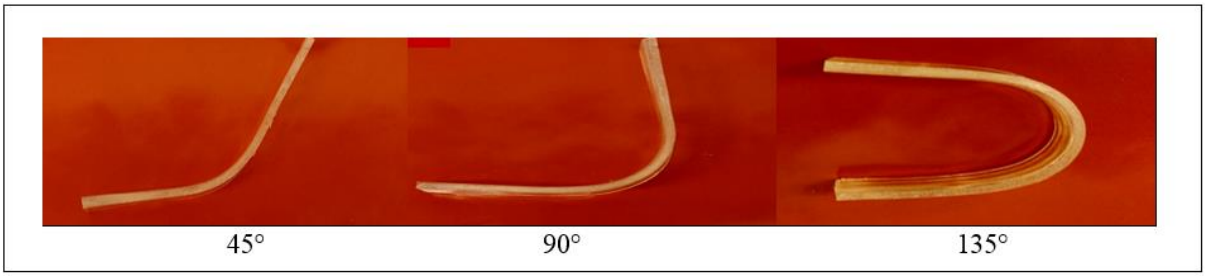

Figure 6.6: SMP deformed under different angles of deformation

The prepared samples were then tested to failure in MTS testing machine to obtain their characteristic mechanical properties as shown in Figure 6.7.

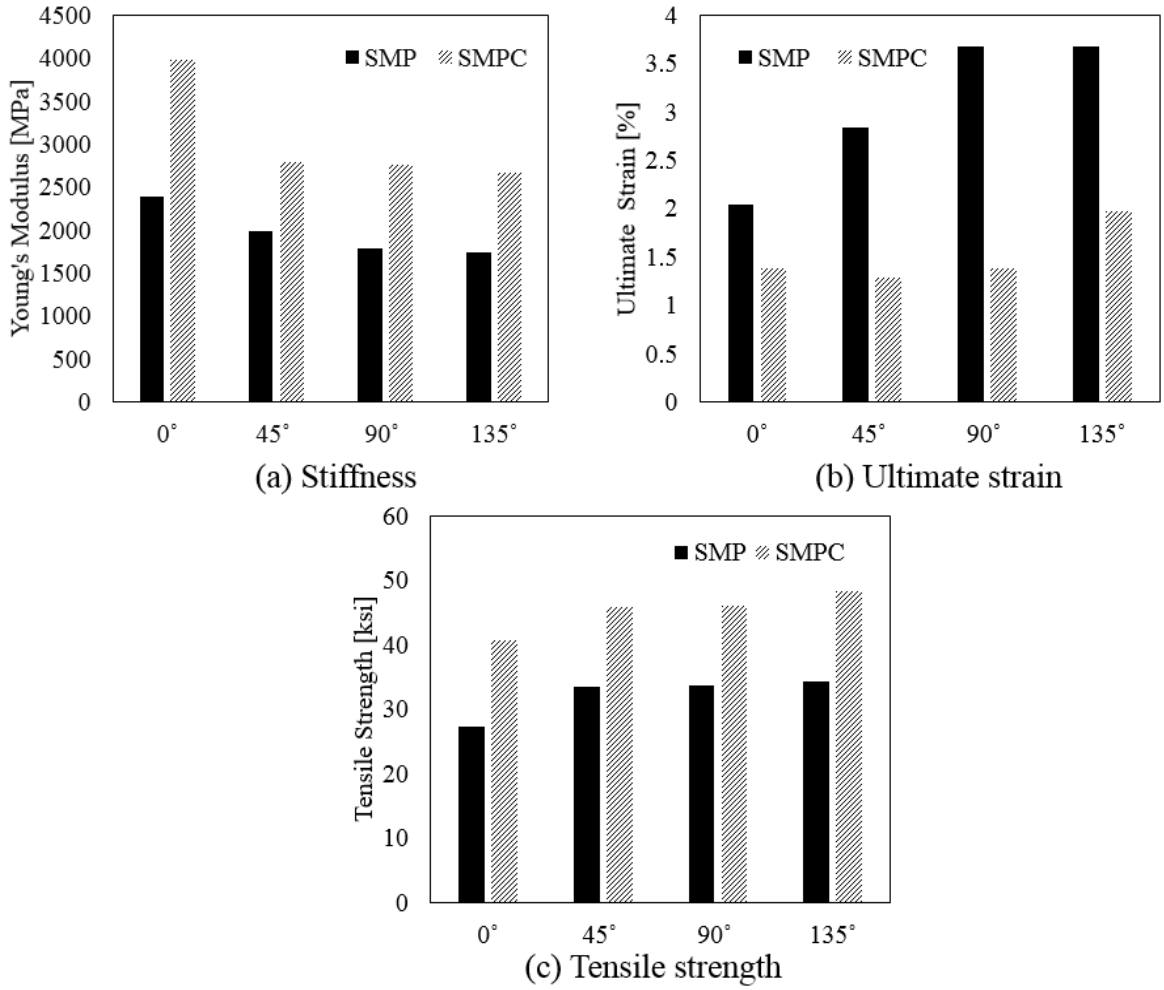

Figure 6.7: Effect of deformation angle on mechanical properties of SMP and SMPC

The bar graph in Figure 6.7 (a) shows the variation of Young's modulus for SMP and SMPC after being deformed under various deformation levels. Quite evidently, the elastic modulus for both SMP and SMPC samples decreased as the deformation angle increased. However, the rate of decrease in stiffness had small dependency on the angle of deformation. The major decline in stiffness (16.58 % for SMP) and (29.87 % for SMPC) occurred after first bending angle deformation of 45°.

Besides, analysing the case with no deformation and the case with 135˚ bending angle deformation, for pure SMP, the percentage decrease in the modulus was calculated to be 36.56% whereas for SMPC the decrease was 45.62%. Furthermore, as expected, the modulus of elasticity for the SMPC was always higher than that of pure SMP. Comparing SMP and SMPC, the maximum increase in stiffness was observed for the samples with no deformation at 67.18% while for the case of 135˚ deformation, the rise was 53.35%. Evidently, as the SMP/SMPC undergoes any level of deformation, the macromolecular chains experience high disorientation and specimen becomes quite flexible, leading to a stiffness decline.

For the case of tensile strain, as the Brownian motion of the specimen increases, the sample becomes flexible and increase in the strain carrying capacity is observed. This may be attributed also to the slackening effect in intermolecular chains found in polyurethane based shape memory polymer products. The tensile strain at failure, comparing specimens with no deformation and samples with 135˚ deformation, the rise was observed to be 44.4% and 30.22% for SMP and SMPC cases, respectively. The maximum strain observed was 3.68% and 1.97% for the SMP and SMPC, respectively, for the 135˚ bending angle deformation case. The ultimate strain for the SMPC samples is

lower than that of the SMP, for all four deformation levels due to the limiting strain carrying capacity of carbon fiber fabric used in manufacturing SMPC.

From the results obtained for tensile strength, as depicted in Figure 6.7 (c), SMPC specimens at all levels of deformation have strengths higher than their SMP counterparts. Comparing SMP and SMPC samples, the maximum rise of 48 % is for samples with no deformation. However, with the increasing degree of deformation, the percentage rise between SMP and SMPC decreases, like for the 135° bending case, the difference in tensile strength between SMPC and SMP is merely 40%. When individually comparing the SMP and SMPC specimens, the tensile strength increases compared to the as-built case (22 % and 13 % for SMP and SMPC, respectively) with 45° bending angle deformation. The value stabilizes after that and no substantial increase is observed with further deformation of 90° and 135° for both SMP and SMPC. Comparing no deformation case and 135° bending case, the tensile strength increases by 25% for SMP case and 19 % for SMPC case, respectively.

CHAPTER 7: CONCLUSIONS

The primary goal of this research was to explore the potential application of unreinforced and carbon-fiber reinforced shape memory polymer for viable structural engineering applications. The shape memory polymer material and its composite was characterized and synthesized in the laboratory as per the glass transition temperature requirements (to be fairly above the ambient temperature range). The material was then thermo-mechanically characterized for its transition temperature using Dynamic Mechanical Analysis. Also, fold deploy tests were conducted to determine shape memory characteristics. Following are the main conclusions were drawn from the study:

- By measuring the peak of the tan δ curve, the T_g of the polyurethane based SMP was found to be 62˚C.
- Excellent shape recovery ratio, close to 98 % was obtained for pure shape memory samples. In addition, shape fixidity obtained was as high as 99 % for the pure SMP samples.
- With the bending deformation angle of 180°, and varying the recovery temperature, ranging it form Tg (62°C), T_g+15 (77 °C) and T_g+30 (92 °C), it was observed that maximum shape recovery ratio (98 %) was independent of the heating temperature. However, rate of shape recovery (and consequently the time to reach equilibrium, permanent shape) increased significantly with the rise of temperature.

The characteristic shape memory cycle consisting of four essential steps of heating (&loading), cooling, unloading and recovery were successfully modelled in Finite Element (FE) framework with temperature dependent elastic modulus and thermal coefficient values and appropriate plastic step definitions. The developed phenomenological model was later successfully applied to the flange of a conventional beam and sufficiently high loading and recovery characteristics were obtained.

Subsequently, the major part of this study explored, the mechanical characteristics of the unreinforced and carbon-fiber fabric reinforced shape memory polymer. Quasi-static tests were performed in a displacement controlled mode and following are the major conclusions that could be successfully inferred from the study:

- Stiffness nearly doubled for SMPC compared to SMP leading to a rise of approximately 100% with the composite having fiber volume fraction of approximately 2%.
- Fracture strain decreased for SMPC samples by approximately 40 % owing to the controlling strain carrying capacity of the carbon fiber.
- The rise in the fracture stress was observed to be close to 50 % which coordinated pretty well with the theoretical predictions.

These results indicated significant improvement in stiffness strength and stiffness improvement in otherwise less stiff shape memory polymer. This could potentially be beneficial in developing shape memory structural components with required stiffness and strength values for different requirements. Subsequently, as the given SMP and its composite are intended to be used for different structural components, it was determined if after undergoing considerable number of shape memory cycles, had any major detriments

to the mechanical strength of the material. In order, mechanical properties of SMP and SMPC were determined after it went through many characteristic shape memory cycles. Following are the key conclusions from the study:

- Stiffness decreased for both SMP and SMPC with the increase in shape memory cycles, with the bending deformation angle of 180°. Notably, the major decline occurred after the first cycle and the ensuing cycles had little to no effect in stiffness degradation.
- Besides, the ultimate strain of SMP increased by as much as 69% after undergoing 4 shape memory cycles compared to as-built case, which is ascribed to the material becoming quite flexible with the increasing number of shape memory cycles. Contradictorily, for SMPC, ultimate strain declined by approximately 16% for the same case scenario.
- The tensile strength was always found to be higher for SMPC compared to SMP, the maximum being for the as-built case with a percentage difference of 48 %. Here also, the major improvement in strength occurred after 1 cycle only and stabilized after a while, accredited to the fact that the deformation and failure govern the first cycle whereas training and memorizing effect govern the subsequent cycles.

The final concluding study evaluated the effect of variance in bending deformation angle ranging from 45° to 135 ° on the mechanical properties of SMP and the composite. The results pertinent to this study can be best summarized as follows:

- With the rise of degree/angle of deformation, comparing as-built and 135° deformation cases, 36.56% decline in stiffness was observed for SMP, whereas for SMPC the decrease was 45.62%. Interestingly, the major decline for both the cases

occurred after 45° deformation and decrease in stiffness had small dependency on the angle of deformation.

- Additionally, with the rise of degree of deformation, the average rise in tensile strength between SMP and SMPC decreased to roughly 40% for 135° case compared to 48% for the no deformation case. As the drop is not that significant, the SMP can be deformed to higher deformation angles without sizeable loss of strength.

REFERENCES

[1] Arnebold, A., & Hartwig, A. (2016). Fast switchable, epoxy based shape-memory polymers with high strength and toughness. *Polymer, 83*, 40-49. doi:http://doi.org/10.1016/j.polymer.2015.12.007

[2] Asaka, K., Oguro, K., Nishimura, Y., Mizuhata, M., & Takenaka, H. (1995). Bending of polyelectrolyte membrane–platinum composites by electric stimuli I. Response characteristics to various waveforms. *Polymer Journal, 27*(4), 436-440.

[3] Baghani, M., & Taheri, A. (2015). An analytic investigation on behavior of smart devices consisting of reinforced shape memory polymer beams. *Journal of Intelligent Material Systems and Structures, 26*(11), 1385-1394.

[4] Barot, G., & Rao, I. (2006). Constitutive modeling of the mechanics associated with crystallizable shape memory polymers. *Zeitschrift für Angewandte Mathematik und Physik (ZAMP), 57*(4), 652-681.

[5] Behl, M., & Lendlein, A. (2007). Shape-memory polymers. *Materials today, 10*(4), 20-28.

[6] Buckley, P. R., McKinley, G. H., Wilson, T. S., Small, W., Benett, W. J., Bearinger, J. P., McElfresh, M. W., & Maitland, D. J. (2006). Inductively heated shape memory polymer for the magnetic actuation of medical devices. *IEEE transactions on biomedical engineering, 53*(10), 2075-2083.

[7] Cadek, M., Coleman, J., Barron, V., Hedicke, K., & Blau, W. (2002). Morphological and mechanical properties of carbon-nanotube-reinforced semicrystalline and amorphous polymer composites. *Applied Physics Letters, 81*(27), 5123-5125.

[8] Cai, W., Meng, X., & Zhao, L. (2005). Recent development of TiNi-based shape memory alloys. *Current Opinion in Solid State and Materials Science, 9*(6), 296-302.

[9] Chae Jung, Y., Hwa So, H., & Whan Cho, J. (2006). Water‐Responsive Shape Memory Polyurethane Block Copolymer Modified with Polyhedral Oligomeric Silsesquioxane. *Journal of Macromolecular Science, Part B, 45*(4), 453-461.

[10] Chang, L., & Read, T. (1951). Plastic deformation and diffusionless phase changes in metals—the gold–cadmium beta phase. *Trans. Aime, 189*(1), 47-52.

[11] Chen, S., Chen, Y., Zhang, Z., Liu, Y., & Leng, J. (2014). Experiment and analysis of morphing skin embedded with shape memory polymer composite tube. *Journal of Intelligent Material Systems and Structures, 25*(16), 2052-2059.

[12] Chen, Y.-C., & Lagoudas, D. C. (2008). A constitutive theory for shape memory polymers. Part II: a linearized model for small deformations. *Journal of the Mechanics and Physics of Solids, 56*(5), 1766-1778.

[13] Chiellini, E., Cinelli, P., Ilieva, V. I., & Martera, M. (2008). Biodegradable thermoplastic composites based on polyvinyl alcohol and algae. *Biomacromolecules, 9*(3), 1007-1013.

[14] Chung, T., Romo-Uribe, A., & Mather, P. T. (2008). Two-way reversible shape memory in a semicrystalline network. *Macromolecules, 41*(1), 184-192.

[15] Coleman, J. N., Khan, U., Blau, W. J., & Gun'ko, Y. K. (2006). Small but strong: a review of the mechanical properties of carbon nanotube–polymer composites. *Carbon, 44*(9), 1624-1652.

[16] Costantino, U., Bugatti, V., Gorrasi, G., Montanari, F., Nocchetti, M., Tammaro, L., & Vittoria, V. (2009). New Polymeric Composites Based on Poly (ϵ-caprolactone) and Layered Double Hydroxides Containing Antimicrobial Species. *ACS applied materials & interfaces, 1*(3), 668-677.

[17] Dassault Systémes. (2014). Documentation Version 6.14-2. *Dassault Systémes Simulia Corp., Providence, RI,USA.*

[18] Ding, H., Liu, X.-M., Wan, M., & Fu, S.-Y. (2008). Electromagnetic functionalized cage-like polyaniline composite nanostructures. *The Journal of Physical Chemistry B, 112*(31), 9289-9294.

[19] Dong, Z. Z., Zhou, S. L., & Liu, W. X. (2001). *A study of NiTiNb shape-memory alloy pipe-joint with improved properties.* Paper presented at the Materials Science Forum.

[20] Duerig, T., Melton, K., & Proft, J. (1990). Wide hysteresis shape memory alloys. *Engineering aspects of shape memory alloys*, 130-136.

[21] Endo, M., Kim, Y., Hayashi, T., Yanagisawa, T., Muramatsu, H., Ezaka, M., Terrones, H., Terrones, M., & Dresselhaus, M. (2003a). Microstructural changes induced in "stacked cup" carbon nanofibers by heat treatment. *Carbon, 41*(10), 1941-1947.

[22] Endo, M., Kim, Y. A., Ezaka, M., Osada, K., Yanagisawa, T., Hayashi, T., Terrones, M., & Dresselhaus, M. S. (2003b). Selective and efficient impregnation of metal nanoparticles on cup-stacked-type carbon nanofibers. *Nano Letters, 3*(6), 723-726.

[23] Gall, K., Dunn, M. L., Liu, Y., Finch, D., Lake, M., & Munshi, N. A. (2002). Shape memory polymer nanocomposites. *Acta Materialia, 50*(20), 5115-5126.

[24] Gall, K., Yakacki, C. M., Liu, Y., Shandas, R., Willett, N., & Anseth, K. S. (2005). Thermomechanics of the shape memory effect in polymers for biomedical applications. *Journal of Biomedical Materials Research Part A, 73*(3), 339-348.

[25] Gomes, M. E., & Reis, R. (2004). Biodegradable polymers and composites in biomedical applications: from catgut to tissue engineering. Part 1 Available systems and their properties. *International materials reviews, 49*(5), 261-273.

[26] Gu, S. (2013). *Effects of Polybenzoxazine on Properties of Shape-Memory Polyurethanes with Glassy and Crystalline Soft Segments.* University of Akron.

[27] Guo, J., Wang, Z., Tong, L., Lv, H., & Liang, W. (2015). Shape memory and thermo-mechanical properties of shape memory polymer/carbon fiber composites. *Composites Part A: Applied Science and Manufacturing, 76*, 162-171.

[28] Hannula, S. P., Söderberg, O., Jämsä, T., & Lindroos, V. (2006). *Shape memory alloys for biomedical applications.* Paper presented at the Advances in Science and Technology.

[29] Hasobe, T., Murata, H., & Kamat, P. V. (2007). Photoelectrochemistry of stacked-cup carbon nanotube films. Tube-length dependence and charge transfer with excited porphyrin. *The Journal of Physical Chemistry C, 111*(44), 16626-16634.

[30] Hayashi, S. (1992). Shape memory polyurethane elastomer molded article: Google Patents.

[31] He, Z., Satarkar, N., Xie, T., Cheng, Y. T., & Hilt, J. Z. (2011). Remote controlled multishape polymer nanocomposites with selective radiofrequency actuations. *Advanced Materials, 23*(28), 3192-3196.

[32] Hu, J. (2013). *Advances in shape memory polymers*: Elsevier.

[33] Hu, J., Zhu, Y., Huang, H., & Lu, J. (2012). Recent advances in shape–memory polymers: Structure, mechanism, functionality, modeling and applications. *Progress in Polymer Science, 37*(12), 1720-1763.

[34] Huang, W., Yang, B., An, L., Li, C., & Chan, Y. (2005). Water-driven programmable polyurethane shape memory polymer: demonstration and mechanism. *Applied Physics Letters, 86*(11), 114105.

[35] Hussain, F., Hojjati, M., Okamoto, M., & Gorga, R. E. (2006). Polymer-matrix nanocomposites, processing, manufacturing, and application: an overview. *Journal of composite materials, 40*(17), 1511-1575.

[36] Jaffe, B. (2012). *Piezoelectric ceramics* (Vol. 3): Elsevier.

[37] Jiang, H., Kelch, S., & Lendlein, A. (2006). Polymers move in response to light. *Advanced Materials, 18*(11), 1471-1475.

[38] Khanolkar, M., Sodhi, J., & Rao, I. J. (2010). *Modeling the Behavior of Crystallizable Shape Memory Polymers Subject to Inhomogeneous Deformations.* Paper presented at the ASME 2010 Conference on Smart Materials, Adaptive Structures and Intelligent Systems: American Society of Mechanical Engineers.

[39] Koerner, H., Price, G., Pearce, N. A., Alexander, M., & Vaia, R. A. (2004). Remotely actuated polymer nanocomposites—stress-recovery of carbon-nanotube-filled thermoplastic elastomers. *Nature materials, 3*(2), 115-120.

[40] Kommareddi, N. S., Tata, M., John, V. T., McPherson, G. L., Herman, M. F., Lee, Y.-S., O'Connor, C. J., Akkara, J. A., & Kaplan, D. L. (1996). Synthesis of superparamagnetic polymer− ferrite composites using surfactant microstructures. *Chemistry of materials, 8*(3), 801-809.

[41] Kumar, U. N., Kratz, K., Wagermaier, W., Behl, M., & Lendlein, A. (2010). Non-contact actuation of triple-shape effect in multiphase polymer network nanocomposites in alternating magnetic field. *Journal of Materials Chemistry, 20*(17), 3404-3415.

[42] Lagoudas, D. C. (2008). *Shape memory alloys: modeling and engineering applications*: Springer Science & Business Media.

[43] Lan, X., Liu, Y., Lv, H., Wang, X., Leng, J., & Du, S. (2009). Fiber reinforced shape-memory polymer composite and its application in a deployable hinge. *Smart materials and structures, 18*(2), 024002.

[44] Langer, R. S., & Lendlein, A. (2002). Shape memory polymers: Google Patents.

[45] Lendlein, A. (2010). *Shape-memory polymers* (Vol. 226): Springer.

[46] Lendlein, A., Jiang, H., Jünger, O., & Langer, R. (2005). Light-induced shape-memory polymers. *nature, 434*(7035), 879-882.

[47] Lendlein, A., & Kelch, S. (2002). Shape ‐ memory polymers. *Angewandte Chemie International Edition, 41*(12), 2034-2057.

[48] Lendlein, A., & Langer, R. (2002). Biodegradable, elastic shape-memory polymers for potential biomedical applications. *Science, 296*(5573), 1673-1676.

[49] Leng, J., Lan, X., Liu, Y., & Du, S. (2011). Shape-memory polymers and their composites: stimulus methods and applications. *Progress in Materials Science, 56*(7), 1077-1135.

[50] Leng, J., Lv, H., Liu, Y., & Du, S. (2008). Synergic effect of carbon black and short carbon fiber on shape memory polymer actuation by electricity. *Journal of Applied Physics, 104*(10), 104917.

[51] Li, F., Liu, L., Lan, X., Zhou, X., Bian, W., Liu, Y., & Leng, J. (2016). Preliminary design and analysis of a cubic deployable support structure based on shape memory polymer composite. *International Journal of Smart and Nano Materials, 7*(2), 106-118.

[52] Li, M. H., Keller, P., Li, B., Wang, X., & Brunet, M. (2003). Light‐Driven Side‐On Nematic Elastomer Actuators. *Advanced Materials, 15*(7‐8), 569-572.

[53] Liang, C., Rogers, C., & Malafeew, E. (1997). Investigation of shape memory polymers and their hybrid composites. *Journal of Intelligent Material Systems and Structures, 8*(4), 380-386.

[54] Liu, C., Qin, H., & Mather, P. (2007). Review of progress in shape-memory polymers. *Journal of Materials Chemistry, 17*(16), 1543-1558.

[55] Liu, F., & Urban, M. W. (2010). Recent advances and challenges in designing stimuli-responsive polymers. *Progress in Polymer Science, 35*(1), 3-23.

[56] Liu, N., Shi, M.-M., Pan, X.-W., Qiu, W.-M., Zhu, J.-H., He, H.-P., Chen, H.-Z., & Wang, M. (2008). Photoinduced electron transfer and enhancement of photoconductivity in silicon nanoparticles/perylene diimide composites in a polymer matrix. *The Journal of Physical Chemistry C, 112*(40), 15865-15869.

[57] Liu, Y., Du, H., Liu, L., & Leng, J. (2014). Shape memory polymers and their composites in aerospace applications: a review. *Smart materials and structures, 23*(2), 023001.

[58] Liu, Y., Gall, K., Dunn, M. L., Greenberg, A. R., & Diani, J. (2006). Thermomechanics of shape memory polymers: uniaxial experiments and constitutive modeling. *International Journal of Plasticity, 22*(2), 279-313.

[59] Liu, Y., Han, C., Tan, H., & Du, X. (2010). Thermal, mechanical and shape memory properties of shape memory epoxy resin. *Materials Science and Engineering: A, 527*(10), 2510-2514.

[60] Lu, G., Tang, H., Qu, Y., Li, L., & Yang, X. (2007). Enhanced electrical conductivity of highly crystalline polythiophene/insulating-polymer composite. *Macromolecules, 40*(18), 6579-6584.

[61] Mather, P. T., Luo, X., & Rousseau, I. A. (2009). Shape memory polymer research. *Annual Review of Materials Research, 39*, 445-471.

[62] Miyazaki, S. (1999). Medical and dental applications of shape memory alloys. *Shape memory materials, 12*, 267-281.

[63] Mohr, R., Kratz, K., Weigel, T., Lucka-Gabor, M., Moneke, M., & Lendlein, A. (2006). Initiation of shape-memory effect by inductive heating of magnetic nanoparticles in thermoplastic polymers. *Proceedings of the National Academy of Sciences of the United States of America, 103*(10), 3540-3545.

[64] Mondal, S., & Hu, J. (2006). Thermal degradation study of functionalized MWNT reinforced segmented polyurethane membrane. *Journal of Elastomers & Plastics, 38*(3), 261-271.

[65] Nguyen, H. (2012). Characterization of Star-shaped marcomolecules with calix [8] arene core by Differential Scanning Calorimetry (DSC).

[66] Nguyen, T. D., Qi, H. J., Castro, F., & Long, K. N. (2008). A thermoviscoelastic model for amorphous shape memory polymers: incorporating structural and stress relaxation. *Journal of the Mechanics and Physics of Solids, 56*(9), 2792-2814.

[67] Ni, Q.-Q., Ohsako, N., Sakaguchi, M., Kurashiki, K., & Iwamoto, M. (2000). Mechanical properties of smart composites based on shape memory polymer. *JCOM: JSMS COMPOSITES-29 of the society of Material Science, Japan,(2000-3), 293*.

[68] Otsuka, K., & Ren, X. (1999). Recent developments in the research of shape memory alloys. *Intermetallics, 7*(5), 511-528.

[69] Perkin Elmer. (2013). Dynamic Mechanical Analysis (DMA): A Beginner's Guide.

[70] Pons, J., Rocon, E., Forner-Cordero, A., & Moreno, J. (2007). Biomedical instrumentation based on piezoelectric ceramics. *Journal of the European Ceramic Society, 27*(13), 4191-4194.

[71] Qiu, Y., & Park, K. (2001). Environment-sensitive hydrogels for drug delivery. *Advanced drug delivery reviews, 53*(3), 321-339.

[72] Ravindranath, R., Ajikumar, P. K., Muhammad Hanafiah, N. B., Knoll, W., & Valiyaveettil, S. (2006). Synthesis and Characterization of Luminescent Conjugated Polymer− Silica Composite Spheres. *Chemistry of materials, 18*(5), 1213-1218.

[73] Sainz, R., Small, W. R., Young, N. A., Vallés, C., Benito, A. M., Maser, W. K., & in het Panhuis, M. (2006). Synthesis and properties of optically active polyaniline carbon nanotube composites. *Macromolecules, 39*(21), 7324-7332.

[74] Schetky, L. (1994). McD," The Current Status Of Industrial Applications For Shape Memory Alloys,". *Trans. of the Mater. Research Soc. of Japan, 18*, 1131.

[75] Schmidt, A. M. (2006). Electromagnetic activation of shape memory polymer networks containing magnetic nanoparticles. *Macromolecular Rapid Communications, 27*(14), 1168-1172.

[76] Scott, T. F., Draughon, R. B., & Bowman, C. N. (2006). Actuation in crosslinked polymers via photoinduced stress relaxation. *Advanced Materials, 18*(16), 2128-2132.

[77] Shape Memory Polymer Properties. (2016). Retrieved from http://www2.smptechno.com/en/smp/

[78] Sokolowski, W., Metcalfe, A., Hayashi, S., Yahia, L. H., & Raymond, J. (2007). Medical applications of shape memory polymers. *Biomedical Materials, 2*(1), S23.

[79] Souri, M. (2014). *Finite element modeling and fabrication of an SMA-SMP shape memory composite actuator*: University of Kentucky.

[80] Stice, J. (1990). The use of superelasticity in guidewires and arthroscopic instrumentation. *Butterworth-Heinemann, Engineering Aspects of Shape Memory Alloys(UK), 1990*, 483-487.

[81] Takeda, T., Shindo, Y., & Narita, F. (2015). Flexural stiffness variations of woven carbon fiber composite/shape memory polymer hybrid layered beams. *Journal of composite materials, 49*(2), 209-216.

[82] Tobushi, H., Hashimoto, T., Ito, N., Hayashi, S., & Yamada, E. (1998). Shape fixity and shape recovery in a film of shape memory polymer of polyurethane series. *Journal of Intelligent Material Systems and Structures, 9*(2), 127-136.

[83] Tobushi, H., Okumura, K., Hayashi, S., & Ito, N. (2001). Thermomechanical constitutive model of shape memory polymer. *Mechanics of Materials, 33*(10), 545-554.

[84] Valasek, J. (1921). Piezo-electric and allied phenomena in Rochelle salt. *Physical review, 17*(4), 475.

[85] Volk, B. L., Lagoudas, D. C., & Chen, Y.-C. (2010). Analysis of the finite deformation response of shape memory polymers: II. 1D calibration and numerical implementation of a finite deformation, thermoelastic model. *Smart materials and structures, 19*(7), 075006.

[86] Wang, L., Rong, L., Yan, D., Jiang, Z., & Li, Y. (2005). DSC study of the reverse martensitic transformation behavior in a shape memory alloy pipe-joint. *Intermetallics, 13*(3), 403-407.

[87] Wax, S., Fischer, G., & Sands, R. (2003). The past, present, and future of DARPA's investment strategy in smart materials. *JOM Journal of the Minerals, Metals and Materials Society, 55*(12), 17-23.

[88] Wei, Z., Sandstroröm, R., & Miyazaki, S. (1998). Shape-memory materials and hybrid composites for smart systems: Part I Shape-memory materials. *Journal of Materials Science, 33*(15), 3743-3762.

[89] Xie, T. (2010). Tunable polymer multi-shape memory effect. *nature, 464*(7286), 267-270.

[90] Xie, T. (2011). Recent advances in polymer shape memory. *Polymer, 52*(22), 4985-5000.

[91] Yang, B., Huang, W., Li, C., Li, L., & Chor, J. (2005). Qualitative separation of the effects of carbon nano-powder and moisture on the glass transition temperature of polyurethane shape memory polymer. *Scripta Materialia, 53*(1), 105-107.

[92] Yang, Z., Herd, G. A., Clarke, S. M., Tajbakhsh, A. R., Terentjev, E. M., & Huck, W. T. (2006). Thermal and UV shape shifting of surface topography. *Journal of the American Chemical Society, 128*(4), 1074-1075.

[93] Yoneyama, T., & Miyazaki, S. (2008). *Shape memory alloys for biomedical applications*: Elsevier.

[94] Yu, K., Liu, Y., Liu, Y., Peng, H.-X., & Leng, J. (2014). Mechanical and shape recovery properties of shape memory polymer composite embedded with cup-stacked carbon nanotubes. *Journal of Intelligent Material Systems and Structures, 25*(10), 1264-1275.

[95] Yu, K., Zhang, Z., Liu, Y., & Leng, J. (2011). Carbon nanotube chains in a shape memory polymer/carbon black composite: to significantly reduce the electrical resistivity. *Applied Physics Letters, 98*(7), 074102.

[96] Zhao, Q., Qi, H. J., & Xie, T. (2015). Recent progress in shape memory polymer: New behavior, enabling materials, and mechanistic understanding. *Progress in Polymer Science, 49–50*, 79-120. doi:http://doi.org/10.1016/j.progpolymsci.2015.04.001